



Accelerating the next technology revolution.

Thickness and Composition Reference Standards for Semiconductor Metrology

Supplier or SEMATECH Confidential
Technology Transfer #11035149A-TR

Advanced Materials Research Center, AMRC, International SEMATECH Manufacturing Initiative, and ISMI are servicemarks of SEMATECH, Inc. **SEMATECH** and the **SEMATECH** logo are registered servicemarks of SEMATECH, Inc. All other servicemarks and trademarks are the property of their respective owners.

**Thickness and Composition Reference Standards for Semiconductor
Metrology
Technology Transfer #11035149A-TR
Supplier or SEMATECH Confidential
July 22, 2011**

Abstract: This report from the MET16 project describes tests of X-ray reflectometry (XRR), X-ray diffraction (XRD), X-ray photoelectron spectroscopy (XPS), and atom probe tomography (APT) for thickness and compositional reference metrology.

Keywords: Measuring Instruments, Spectroscopy, Standard Artifacts, Standard Reference Material, Thin Film Thickness, X-ray Diffraction, X-ray Reflectometry

Authors: Victor Vartanian, Donald Windover and David Gil (NIST), Tom Kelly (Cameca Instruments), and Tom Larson (Revera)

Approvals: Victor Vartanian, Project Manager
Phil Bryson, Director
Laurie Modrey, Technology Transfer Team Leader

Table of Contents

1	EXECUTIVE SUMMARY	1
2	MOTIVATION FOR REFERENCE STANDARDS	1
3	CONSIDERATIONS FOR REFERENCE STANDARD DEVELOPMENT	2
	3.1 Calibration Artifact	2
	3.2 Instrumentation and Data Collection	2
	3.3 Theory and Data Analysis	3
4	CURRENT REFERENCE STANDARDS FOR THE SEMICONDUCTOR INDUSTRY	3
	4.1 Thickness Reference Wafers	3
	4.2 Composition Reference Wafers	4
	4.2.1 NIST Standard Reference Materials	4
	4.2.2 Reference Standards Fabricated at CNSE	4
	4.3 Optimal NIST-Traceable Test Artifacts for Thickness Metrology	5
	4.3.1 Single Layer vs. Multilayer Test Structures	6
	4.3.2 Effect of Surface Roughness	6
	4.4 Status of SEMATECH-NIST XRR Standard Reference Material Development	6
	4.4.1 Suitability of XRR for Thickness Metrology	6
	4.4.2 Composition Metrology	7
	4.4.3 Considerations for Composition Metrology	7
	4.4.4 Rutherford Backscattering Spectroscopy (RBS)	7
	4.4.5 Suitability of XPS for Thickness and Composition Reference Metrology	8
	4.4.6 XPS Quantification: Calculating Atomic Compositions for SiO%, O%, N% ..	10
	4.4.7 Suitability of APT for Composition Reference Metrology	12
	4.5 Calibration Artifact Development	14
	4.5.1 Data Analysis and Uncertainty Estimation	17
	4.6 Results from Si ₃ N ₄ Film XRR Data Analysis	21
5	CONCLUSION AND FUTURE DIRECTION	23
	5.1 SEMATECH Reference Wafer Samples	23
	5.2 Discussion	33
	5.3 Conclusions and Outlook	33
6	REFERENCES	33

List of Figures

Figure 1	XRD Plot of SiGe on Bulk Si.....	3
Figure 2	Film Thickness Variance at Shallow X-ray Beam Angles.....	6
Figure 3	Photoelectron Attenuation Limits Measurement to Top 10 nm of a Sample	9
Figure 4	Calculation of Film Thickness Depends on Peak Intensity as Well as Differences in Mean Free Paths of Different Species in Spectra	10
Figure 5	XPS is Capable of Determining Thickness in Multilayer Films	11
Figure 6	SIMS (Blue Curve) Analysis of NIST 2137 Compared with LEAP.....	13
Figure 7	Spatial Distribution Map of a Silicon Specimen Showing the {200} as Horizontal Planes in the Data.....	13
Figure 8	Stages of FIB Specimen Preparation from a) Cutting Trenches to h) Final Tip Shape.....	13
Figure 9	Schematic of the Transistor and Atom Maps from a 20 nm Thick Segment of the Transistor Status of ISMI/SEMATECH-NIST XRR Standard Reference Material Development [10].....	14
Figure 10	Pros and Cons of a Single Layer Structure as an XRR SRM.....	14
Figure 11	Theoretical XRR Data from a 50 nm Si ₃ N ₄ Film on a Si Substrate.....	15
Figure 12	Pros and Cons of a Multilayer Structure as an XRR SRM	16
Figure 13	Theoretical XRR Data from a Three Repeat Bi-Layer Si/GiGe Structure on a Si Substrate.....	16
Figure 14	Data Analysis Method for Refining Physical Parameters to XRR Data	17
Figure 15	Comparison of Genetic Algorithms (optimization-based) vs. Monte Carlo (statistics-based) Data Analysis Methods.....	18
Figure 16	Thickness Probability Distribution for Theoretical 50 nm Si ₃ N ₄ on a Si Calibration Artifact.....	19
Figure 17	Electron Density of a Single Layer of Si ₃ N ₄ on a Si Wafer	20
Figure 18	Electron Density of a Surface and Interface Layer for Si ₃ N ₄ on a Si Structure	20
Figure 19	Electron Density for a Si ₃ N ₄ Film with a Density Gradient.....	20
Figure 20	Actual XRR Data from a 16 nm Si ₃ N ₄ Film on a Si Substrate	21
Figure 21	Thickness Probability Distribution for One-Layer Markov Chain Monte Carlo Analysis	22
Figure 22	Electron Density for the Eight-Layer Monte Carlo Model of the Actual Si ₃ N ₄ Film Data.....	22
Figure 23	CVD Si ₃ N ₄ Simulated Reflectance Spectrum	24
Figure 24	CVD Si ₃ N ₄ Simulated and Measured Reflectance Spectra.....	24
Figure 25	Topographical Map of 50 nm CVD Si ₃ N ₄ Wafer	25
Figure 26	1-σ Topographical Map of Variation for the 50 nm CVD Si ₃ N ₄ Wafer	26

Figure 27	81-Point Spectroscopic Ellipsometry Surface Topographical Map of 50 nm CVD Nitride Film.....	26
Figure 28	XRR Measured and Theoretical Reflectance Spectra Using a Three-Layer Model	27
Figure 29	XRR Measured and Theoretical Reflectance Spectra Using an 8-Layer Model	28
Figure 30	25-Point XRR Surface Topographical Map of the 15 nm CVD Nitride Wafer.....	29
Figure 31	1- σ Topographical Map of Variation for the Furnace-Deposited 15 nm Si ₃ N ₄ Wafer	29
Figure 32	Illustration of SiGe Superlattice with Si ₃ N ₄ Cap	30
Figure 33	SiGe Superlattice Simulated Reflectance Spectrum	31
Figure 34	SiGe Superlattice Actual Reflectance Spectrum	31
Figure 35	NIST-proposed Structure for Combined X-ray and TEM Calibration with Si/Si(1-x)Ge _x Strained Superlattices.....	32

List of Tables

Table 1	Boron-Doped SiGe Composition Wafer.....	5
Table 2	HKMG Thickness Wafers	5
Table 3	Thickness Determination Comparison for Furnace Si ₃ N ₄ on Si (nominal 15 nm)	23
Table 4	Three-Layer Regression Model with 10 Parameters Floating	24
Table 5	Results of Three-Layer GA Regression.....	25
Table 6	Three-Layer Regression Model with 10 Parameters Floating	27
Table 7	Eight-Layer Regression Parameter Model with 25 Parameters Floating	28
Table 8	Regression Model with 15 Parameters Floating	30

1 EXECUTIVE SUMMARY

SEMATECH has indicated the need for reference standards for films thickness and composition to improve measurement accuracy and comparisons with complementary measurement techniques. Several metrology techniques were evaluated for their suitability to verify various candidates for thickness and composition standards. The evaluation was based on their ability to measure thickness or composition based on International System of Units (SI) measurement standards of time and distance, using calibration-free techniques.

In 2010, several thickness and composition test structures were developed and the capability to model thickness information from both theoretical structures and deposited thin films was tested. X-ray reflectometry (XRR), X-ray diffraction (XRD), X-ray photoelectron spectroscopy (XPS), and atom probe tomography (APT), with Rutherford backscattering (RBS) and transmission electron microscopy (TEM) as verification techniques, were shown to be the best methods currently available for thickness and compositional reference metrology.

2 MOTIVATION FOR REFERENCE STANDARDS

To enable tool matching, films must be measured with low uncertainty to ensure reproducible measurements across tools at different times and places. Specifications of measurement accuracy are also increasingly important as films are measured in parallel across divergent tool platforms.

A motivation for a standard reference material is to provide companies with National Institute of Standards and Technology (NIST)-traceable reference standards for semiconductor metrology tools. To be NIST-traceable, units of measure must originate from the SI unit of time (the second) or length (the meter). Several analytical techniques can be correlated to a time measurement, such as instruments that count ions or electrons over a given time or instruments that measure atoms using distance as their measurement basis.

Tool health must be monitored on “golden” wafers, using absolute intrinsic or international standards. Having an optimized set of wafers improves tool-to-tool or fleet matching. A certified thickness also allows compensation for airborne molecular contamination (AMC).

For NIST-traceable standards, various uniform, stable, and single- or multiple-layer films need to be created so that XRR or XRD can be used as the primary thickness metrology technique.

For NIST-traceable composition standards, reference standards for different compositions of relevant thin film materials (e.g., B in SiGe, N in SiON, etc.) must be created, followed by compositional analysis using complementary techniques to assess elemental distribution across films (e.g., XPS and APT). In addition, because the reference standard must be immutable, time-dependent studies of the variation of reference wafers should be undertaken.

NIST certifies both reference materials and standards. While standards have direct traceability to a higher authority, references do not, often because there is no official standard. Each type of product is made to a rigorous set of internal specifications and serves as an excellent calibration artifact.

3 CONSIDERATIONS FOR REFERENCE STANDARD DEVELOPMENT

3.1 Calibration Artifact

Wafers need to have well known single or multilayer compositions, with high density contrast between adjacent layers. They also need high center-to-edge thickness uniformity as well as low density variation with respect to depth. For XRR, the film surface and any interfaces need to have minimal roughness to reduce both film thickness uncertainty and diffuse scattering. For multiple film standards, interfaces must be abrupt. The film materials must also be stable over time. Capping layers may be needed to limit exposure of the surface to species that can absorb into or adsorb onto the film. In one SEMATECH-NIST study, film thickness uncertainty was found to be dominated by AMC [1].

3.2 Instrumentation and Data Collection

The measurement tool must have Si-traceable angle and wavelength measurement capability. XRR and XRD are both good candidates for thickness metrology, as each measurement is obtained at a given beam or goniometer angle with an associated intensity. XRR and XRD both rely on a well-defined X-ray wavelength (length), and each measurement is obtained at a specific angle that can be encoded to a reference laser for high accuracy.

The ability to extract compositional information from a measurement of the lattice parameter in a crystal potentially makes XRD a first-principles technique compatible with compositional analysis as a reference metrology tool. For example, Vegard's Law assumes that the distortion of a crystal lattice is linear with the concentration of substitutional Ge atoms in a fully strained crystal. However, if the lattice relaxes, then two effects will contribute to the lattice parameter and the shift in the SiGe layer peak: the composition and the relaxation. For thin, vertically uniform SiGe films below the critical thickness beyond which the lattice relaxes, XRD may be a good method for compositional analysis, with reliance on Vegard's Law and possible finite element analysis of the strain fields. The position of the Ge peak in Figure 1 is a function of only the lattice strain and Ge composition. If the lattice is fully strained, then the Ge peak position is a function of only composition.

XPS can also be used as a composition monitoring standard reference metrology tool because elements are identified by peaks associated with distinct wavelengths, and the ratios of peaks determine the elemental ratios in a material.

In addition, APT may be a potential candidate for a composition reference metrology tool. However, it must be evaluated for this application. The operation of the technique is described in Ref. [2].

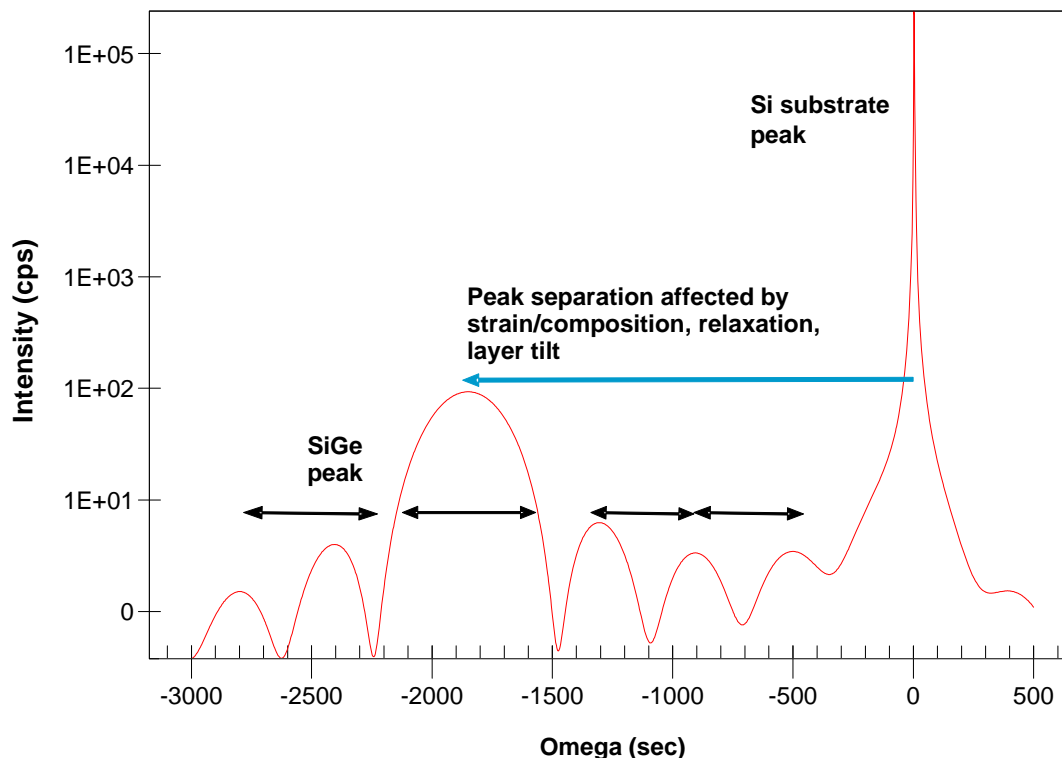


Figure 1 XRD Plot of SiGe on Bulk Si

3.3 Theory and Data Analysis

A first principles structural modeling approach that includes statistical methods for uncertainty analysis of the thickness, roughness, and density of each film layer must be applied using techniques established by NIST. Surface contamination must also be included in the uncertainty analysis since this can often dominate the uncertainty analysis. Interfaces and interdiffusion layers can increase uncertainty in each measurement. Comparison to a TEM cross section is often required to delineate each layer. TEM is especially useful in analyzing thickness because of the ability to distinguish between interfaces and the film of interest.

4 CURRENT REFERENCE STANDARDS FOR THE SEMICONDUCTOR INDUSTRY

4.1 Thickness Reference Wafers

VLSI Standards sells thermally grown SiO₂ wafers (100, 125, 150, 200, and 300 mm) with varied certified thicknesses (2, 4.5, 7.5, 12, 25, 50, 100, 400, 675, and 1010 nm). VLSI Standards also sells plasma enhanced chemical vapor deposited (PECVD) Si₃N₄ wafers (100, 125, 150, and 200 mm) with varied certified thicknesses (20, 90, 400, 120, and 200 nm). The certified area in the wafer center is a 10 mm diameter region.

These wafers are certified using spectroscopic ellipsometry (SE) with wavelengths from 400–700 nm, with the refractive index and extinction coefficient of the Si substrate matching the values stated by NIST. The SE instrument was calibrated using NIST Standard Reference Materials 2532 and 2533.

4.2 Composition Reference Wafers

4.2.1 NIST Standard Reference Materials

A standard reference material was developed for secondary ion mass spectroscopy (SIMS) based on ion implantation of boron into Si (SRM 2137) [3]. A single crystal Si (100) commercial n-type wafer (76 mm diameter), polished on one side, was implanted with ^{28}Si ions in an ion implanter to amorphize the surface before ion-implantation (polished side) with ^{10}B at a nominal energy of 50 keV. A grid of 5 mm squares was patterned on the unpolished side of the wafer. Each grid contains row, column, and wafer numbers for identification. The ^{28}Si ions are implanted in three stages: $2\text{E}+15$ atoms/ cm^2 at 360 keV (as Si^{2+}), $2\text{E}+15$ atoms/ cm^2 at 140 keV (as Si^{1+}); and $2\text{E}+15$ atoms/ cm^2 at 50 keV (as Si^{1+}). The B concentration was certified by a neutron reaction method (i.e., neutron depth profiling) using a calibrated reference film of metallic ^{10}B deposited on Si as a standard. The retained dose of ^{10}B has a $0.01692 \mu\text{g}/\text{cm}^2 \pm 0.00059 \mu\text{g}/\text{cm}^2$ uncertainty. With a value of $10.012937 \text{ g}/\text{mol}$ for the isotopic mass of ^{10}B , the retained dose is equivalent to $1.018\text{E}+15 \text{ at}/\text{cm}^2 \pm 0.035\text{E}+15 \text{ at}/\text{cm}^2$. The wafers were cut into $1 \times 1 \text{ cm}$ squares. All squares were located at least 7 mm from the wafer edge. Before use, dust particles should be removed from the surface with a pressurized duster. Cleaning with HF is not recommended since boron will be consumed within the surface oxide. The grid pattern etched on the back of the samples will also be removed.

4.2.2 Reference Standards Fabricated at CNSE

Several materials were fabricated at the College of Nanoscale Science and Engineering (CNSE) (Table 1), including composition standard candidates of B-doped SiGe, 1.5% SiC, and several high-k metal gate wafers. The patterned B-doped 50 nm SiGe (25 and 30% Ge) wafers were deposited by chemical vapor (CVD) on n-type substrates, with B concentrations of $1\text{E}+18$, $1\text{E}+19$, and $1\text{E}+20 \text{ at}/\text{cm}^2$ and capped with a 10 nm Si using SEMATECH's 461AZ MOSCAP reticle.

Candidates for thickness standards included a SiGe/Si lattice capped with Si_3N_4 and two types of Si_3N_4 wafers (CVD and thermal), tested for their suitability as reference wafers. Ideal B-doped SiGe wafers would have uniform distributions of CVD B and Ge. The advantage of CVD B doping over implant is that the distribution of B is likely to be more uniform.

A set of high-k metal gate (HKMG) wafers (Table 2) was fabricated to test the ability of the metrology techniques, in particular XPS and APT for compositional analysis, on a multi-film stack.

Table 1 Boron-Doped SiGe Composition Wafer

Wafer	Split	% Ge	SiGe Thickness (Å)	Approximate Boron Concentration (at/cm ²)	Si Cap Thickness (nm)
1	1	25	50	1E+18	10
2	1	25	50	1E+18	10
3	1	25	50	1E+18	10
4	1	25	50	1E+18	10
5	2	25	50	1E+19	10
6	2	25	50	1E+19	10
7	2	25	50	1E+19	10
8	2	25	50	1E+19	10
9	3	25	50	1E+20	10
10	3	25	50	1E+20	10
11	3	25	50	1E+20	10
12	3	25	50	1E+20	10
13	4	30	50	1E+18	10
14	4	30	50	1E+18	10
15	4	30	50	1E+18	10
16	4	30	50	1E+18	10
17	4	30	50	1E+18	10
18	4	30	50	1E+18	10
19	4	30	50	1E+18	10
20	5	30	50	1E+19	10
21	5	30	50	1E+19	10
22	5	30	50	1E+19	10
23	5	30	50	1E+19	10

Table 2 HKMG Thickness Wafers

Wafer	Thermal Oxide (nm)	High-k Gate Dielectric (nm) – HfO ₂	Metal Gate Thickness (nm) – TiN
1	2	2	10
2	2	3	10
3	2	4	10
4	2	2	20
5	2	3	20
6	2	4	20

4.3 Optimal NIST-Traceable Test Artifacts for Thickness Metrology

To be a candidate artifact as a standard reference material, the test structure should be a single or multilayer, with high density contrast between adjacent layers, with a known composition, little roughness, and good across-wafer uniformity. It should also be time-invariant.

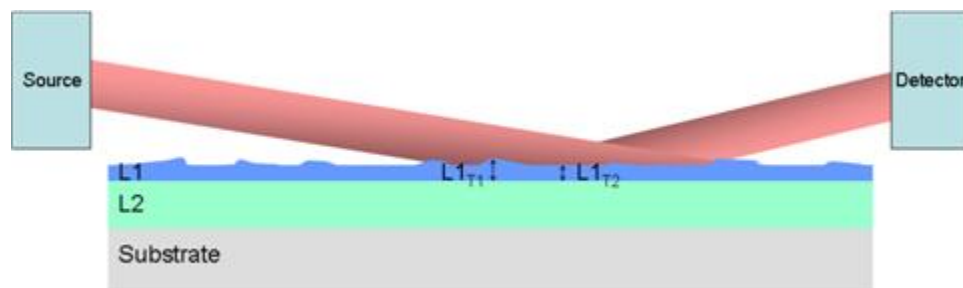
4.3.1 Single Layer vs. Multilayer Test Structures

A single layer structure is the most desirable artifact due to its simpler uncertainty estimate. A single layer artifact enables a first principle model to be used, with roughness and density calculated to include the uncertainty estimation. However, AMC can become the predominant component in the uncertainty analysis. In addition, film interfaces or elemental interdiffusion layers can challenge SI traceability [4].

A multilayer structure dramatically reduces the uncertainty estimates due to layer period spacing. However, the XRR model becomes more complex. As the number of layers increases, the increased number of free parameters (thickness, density, roughness) makes the uncertainty estimate challenging, if not impossible. The quality of the data from individual layers in the structure may also degrade. Finally, any films that exert stress on the wafer will cause wafer bow, increasing uncertainty in the film thickness due to film variation within the X-ray beam. In some cases, wafer backside deposition to compensate for frontside stress and wafer bow must be considered. XRD is sensitive to detecting a curvature of radius as large as 700 m [5].

4.3.2 Effect of Surface Roughness

For measurements at grazing angles, such as XRR, film thickness variance at shallow X-ray beam angles increases error in model since a longer beam must interact with varying film thicknesses (Figure 2).



Note: Increases error in the XRR model due to the longer beam interacting with varying film thicknesses.

Figure 2 Film Thickness Variance at Shallow X-ray Beam Angles

4.4 Status of SEMATECH-NIST XRR Standard Reference Material Development

4.4.1 Suitability of XRR for Thickness Metrology

XRR determines the thickness of a film using interference fringes to characterize the film's structural properties (thickness, density, and roughness). The technique has potential for SI traceability of film thickness measurements. Since XRR theory relies on surface discontinuity, interfaces between layers of similar electron density are not detected. The effects of multiple film layers can be convoluted using a recursive relation attributed to Parratt [6]. Rough interfaces complicate modeling by damping the intensities of interference fringes and reducing the overall reflection intensities. A Gaussian roughness model is assumed for each electron density interface, characterized by the root mean square (RMS) roughness of the film. Parratt recursion for multiple layers and Gaussian roughness modeling for each interface provide simultaneous refinement of the structural properties (e.g., film thickness, t film, and density, r film, s film, etc.).

To obtain reasonable signal intensity, surfaces and interfaces must have high reflectivity/low roughness as well as a minimum ~10% difference in electron density contrast between adjacent layers. Reflectance data must be collected at high angles to capture as many fringes as possible to reduce uncertainty in the thickness measurements. A low noise background and detector threshold also allow more accurate determinations of thickness and roughness.

XRR provides thickness, density and roughness information for thin, smooth, blanket films, which are prevalent in the semiconductor industry. In contrast to other thickness determination techniques such as spectroscopic ellipsometry (SE), XRR can provide a traceable thickness over a range from several nm to nearly 1 μm , if the material layers exhibit sufficient electron density contrast. The technique uses an optical interference phenomenon (Snell's law) to probe information from a single film or a multilayer structure, in much the same way as SE. The advantage with XRR is that the refractive index for X-rays for all materials is nearly 1, hence determining thickness depends only slightly on knowledge of the materials' refractive index.

The technique uses specular reflection of X-rays grazing from the surface of a film, making it the technique best suited for highly uniform and not very rough blanket films. Thin films will act like a single slit diffraction, with the oscillations in intensity providing direct thickness information. For a single layer film, for which the oscillation period is inversely related to thickness, interpretation is straightforward. Fourier transform methods are often used to approximate film thickness. If process monitoring is the goal, then monitoring run-to-run variation of this periodicity will yield thickness variation information.

4.4.2 Composition Metrology

NIST offers a standard reference material (SRM) 2841 to be used as for analytical methods that measure the composition of thin films. Such methods include electron microprobe analysis (EMPA), photoluminescence (PL), auger electron spectroscopy (AES), and XPS. A unit of SRM 2841 consists of a 3 μm thick epitaxial layer of $\text{Al}_x\text{Ga}_{1-x}\text{As}$, grown on GaAs, with Al mole fraction x , nominally 0.20, certified by NIST to within an expanded uncertainty of 0.002 atomic mole fraction or less. The semiconductor piece is approximately 1 cm^2 and is mounted onto a stainless steel disk (for labeling and handling) by adhesive carbon tape. NIST also offers units of SRM 2842 with Al mole fraction near 0.30 [8].

4.4.3 Considerations for Composition Metrology

A first principles metrology technique for composition would allow quantitation either by direct counting of atoms in a matrix or by peak intensity without relying on calibration to a primary standard.

4.4.4 Rutherford Backscattering Spectroscopy (RBS)

RBS, which is useful for determining the thickness and composition of films thicker than 10 nm, does not rely on standards. Elements in a sample can be determined from the positions of the backscattered He^{2+} (alpha particle) or proton peaks in the energy spectrum; depth can be determined from the width and shifted position of these peaks; and relative concentration is determined from peak height. RBS is especially useful for analyzing a multilayer sample or a sample with a composition that varies more continuously with depth. Because no commercial suppliers offer RBS, most are laboratory instruments, hence no further detail is provided here.

4.4.5 Suitability of XPS for Thickness and Composition Reference Metrology

XPS, also known as electron spectroscopy for chemical analysis (ESCA), is a powerful and versatile metrology technique that relies on the ability to measure the binding energies of outermost shell electrons. Spectra are obtained by irradiating a sample with a monochromatic beam of X-rays with simultaneous measurements of the number and kinetic energy of emitted electrons in an ultra-high vacuum environment. Electrons are ejected from all orbitals having a binding energy less than the energy of the X-ray beam, although not with the same probability. Thus, some peaks are more intense than others. Equation 1 shows that the relationship between the measured kinetic energy (KE) of the ejected electron depends on the binding energy E_b , which is material-dependent (ϕ_s is the workfunction of the detector, h is Planck's constant, and λ is the wavelength of the X-ray, typically 0.1541 nm for Cu $K_{\alpha 1}$):

$$E_b = h\nu - KE + \phi_s \quad \text{Eq. [1]}$$

Atomic count directly yields a measurement of atomic concentration or atomic percent. Signal intensity is a function of the elemental concentration, the mean free path of the electron, and the absorption cross section of X-rays on the sample material. As long as these factors are well understood, or if standards are available, good quantification accuracy is possible. The concentration of elements within the sample is obtained from the signal intensity if the signals can be corrected depending on the effects of other materials in the sample. However, for single layers of uniform films, XPS provides stoichiometric information useful for reference metrology.

Sampling depths are on the order of 0.5–2.5 nm for metals and metal oxides and 4–10 nm for organic materials and polymers.

The resulting positively charged surface can be charge-neutralized with a low energy thermal electron flood gun. XPS can also be performed on insulating surfaces. Spot sizes are on the order of 10 μm .

Measurements of binding states allow a material's chemical composition, chemical state (functional groups present), oxidation state (chemical state of an element or material with non-zero charge), and electronic state to be determined. The sensitivity of XPS is generally in the range of 0.1% (5×10^{19} at/cm³). XPS is sensitive to all elements, although hydrogen and helium have such small electron orbital diameters that the cross section is very low. XPS is therefore an excellent technique for monitoring the surfaces of materials in semiconductor devices. One of the chief attributes of XPS is the ability to monitor small shifts in the photoelectron spectrum. These small chemical shifts provide information on the chemical state of detected elements when compared to the peak positions of pure elements. In some cases, chemical shifts may be as much as 1–10 eV, in other cases as little as only a few tenths of an eV. When chemical shifts are in this range, calibration of the instrumental binding energy (BE) scale must be better than 0.1 eV. Various methods for determining binding energies have been developed. NIST has developed a method for energy scale calibration [7] based on the metal used as a calibrant, primarily gold, silver, or copper. Tables of atomic binding energies are available at <http://cxro.lbl.gov/PDF/X-Ray-Data-Booklet.pdf>.

Additional measurements are modeled based on a model of the film stack and the way photoelectrons interact with the atoms in the film stack before leaving the sample and being detected. A model includes a set of assumptions about the film stack. If the physical reality is different from the model assumptions, then some systematic, but known, errors will occur in the measurement. In this way, both thickness and dose are modeled.

X-rays penetrate several microns into the sample. Photoelectrons are emitted throughout the penetration depth, but only those generated near the surface escape and are detected. In the example shown in Figure 3, $KE_0 > KE_1 > KE_2 > KE_3 > KE_4 > KE_5$ as the photoelectron loses energy through inelastic collisions in the sample. Of the photoelectrons generated “deep” in the sample, most are not detected; e.g. at approximately 10 nm deep, >95% do not escape.

As shown in Figure 4, photoelectrons emitted by the substrate Si atoms must travel through the SiON film before leaving the surface. Only those electrons without energy loss can leave the sample and contribute to the XPS peak. Photoelectrons that lose energy will no longer be detected at the characteristic peak position. Thicker SiON film results in fewer electrons detected from bulk Si atoms.

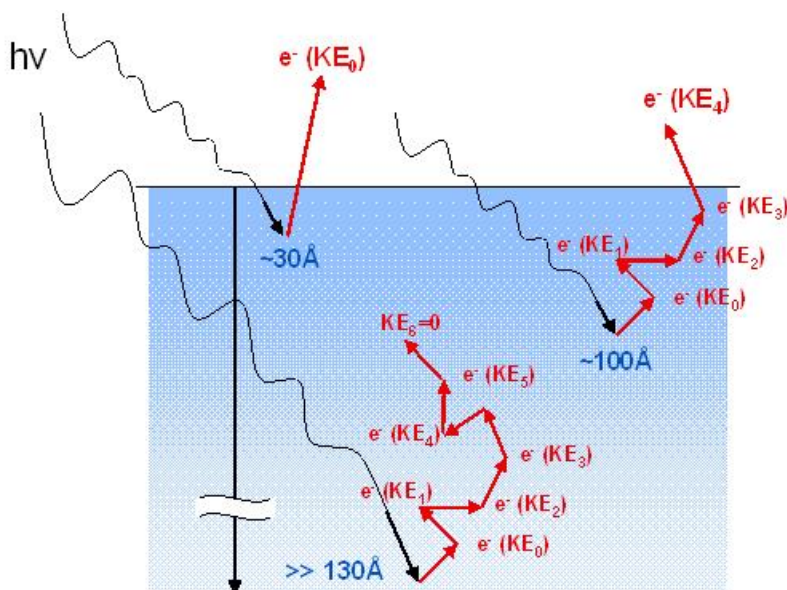


Figure 3 Photoelectron Attenuation Limits Measurement to Top 10 nm of a Sample

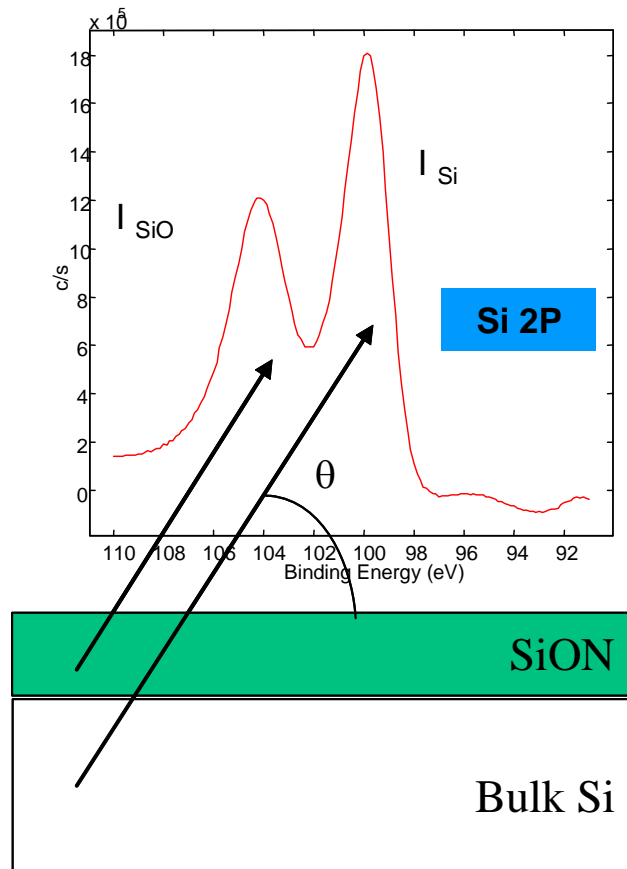


Figure 4 Calculation of Film Thickness Depends on Peak Intensity as Well as Differences in Mean Free Paths of Different Species in Spectra

$$d \propto f \left(\frac{I_{SiO}}{I_{Si}}, K, \lambda, \theta \right)$$

where: d is the SiON film thickness
 I_x is the XPS intensity of species X (SiO or Si)
 K is a materials constant
 λ is the effective attenuation length
 θ is the angle between the sample surface plane and the electron analyzer axis

4.4.6 XPS Quantification: Calculating Atomic Compositions for SiO%, O%, N%

Elemental compositions within a film can be quantified by normalizing the extracted intensities by appropriate atomic sensitivity factors. For example, SiO%, O%, and N% elemental compositions are calculated by renormalizing by the sum of the normalized intensities. By definition, the SiO%, O%, and N% add up to 100%. A set of equations Eq. [2]–Eq. [4] that determine the composition of species in a SiON film relies on the intensity of each peak. A correction is made using the atomic sensitivity factor.

$$N\% = \frac{I_{\text{Nitrogen}} / ASF_N}{\sum_n \frac{I_n}{ASF_n}} \times 100 \quad \text{Eq. [2]}$$

$$O\% = \frac{I_{\text{Oxygen}} / ASF_O}{\sum_n \frac{I_n}{ASF_n}} \times 100 \quad \text{Eq. [3]}$$

$$SiO\% = \frac{I_{\text{Silicon-O}} / ASF_{Si-O}}{\sum_n \frac{I_n}{ASF_n}} \times 100 \quad \text{Eq. [4]}$$

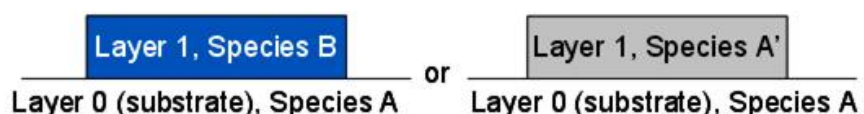
where: $SiO\%$: Composition of SiO
 $O\%$: Composition of O
 $N\%$: Composition of N
 I_x : XPS Intensity of element x
 $ASF(x)$: Atomic sensitivity factor for x

Some other film systems that can be used are shown in Figure 5. Each total film stack must be less than 10 nm thick. The ability to determine thickness from these models assumes good intensity extraction for species A, B, C, and no overlapping peaks; furthermore, species A, B, and C are assumed to be unique to one layer. Thus, for thicker films, RBS may be a better solution.

Because XPS relies on the ratios of independent spectral peaks, XPS shows promise as a stable and accurate reference metrology method for thin films comprised of multiple and varying compositions.

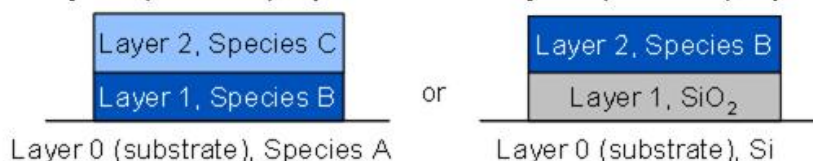
Single Layer

eg. SiO(N)/Si, Al₂O₃/TiN, HfSiO(N)/Si



Two Layer Film

eg. HfO/SiO/Si, TiN/Al₂O₃/Si, HfAlO/SiO/Si



Three Layer Film

eg. HfO₂/Al₂O₃/SiO₂/Si, Al₂O₃/HfO₂/SiO₂/Si

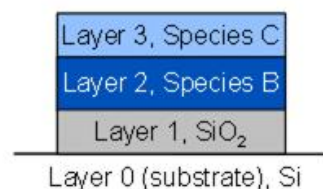


Figure 5 XPS is Capable of Determining Thickness in Multilayer Films

4.4.7 Suitability of APT for Composition Reference Metrology

APT complements TEM and SIMS. It delivers 3D reconstructions of atom positions and identities using point-projection microscopy onto a position-sensitive detector to determine the lateral position of atoms in a sample coupled with time-of-flight spectroscopy to identify atoms. The spatial resolution of APT has been reported to be as high as ~0.2 nm, with an atomic sensitivity as high as <10 atomic parts per million (appm). Detection efficiency is >50%, and all elements are detected with equal efficiency.

Field evaporation is used to remove atoms from a specimen by ionizing an atom on the specimen surface under a high electric field (10^{10} V/m); the resultant ion is accelerated toward the counter electrode (detector) by the high field. Specimens are cooled to 20° to 80° K to freeze the surface migration of atoms. A needle-shaped specimen is required to both create the high fields and give the point-projection magnification of the image. All atoms are field-evaporated from the apex of a specimen in an atom probe. Neutral atoms ejected from the surface are considered negligible, which means that the ionization probability is essentially 100%. The atom identities are determined by time-of-flight mass spectroscopy during which field evaporation events are pulsed in short time windows (<1 ns) by pulsing either the electric field or specimen apex temperature (with a laser). Experiments must be performed such that the integrated evaporation probability between pulses (the off cycle) is negligible compared to the probability during pulses (the on cycle). In general, assuming that these conditions are met, which is not too difficult for most materials, then all atoms are evaporated only during on cycles and are correctly analyzed. An instrument could be run under conditions that produce erroneous composition measurements by failing to meet the above criterion, but this can normally be avoided.

Composition is determined by adding up all the atoms in a given volume. Errors occur when any one element is preferentially detected. Such error sources include a) preferential out-of-pulse evaporation of one or more elements (they fail to be detected as time-correlated events) and b) preferential detection of one or more elements. For example, analyzing certain compound semiconductors requires great care because the column V atoms (N, P, As, ...) are more prone to evaporation between pulses than the column III atoms (Ga, In, ...). Also, some dopant elements in silicon (particularly B) will cluster on the surface and evaporate in small bursts, creating a detection challenge for multiple events from one pulse. These types of complications are mostly understood and alleviated in careful analysis work. The data in Figure 6 compare SIMS results on the NIST SRM 2134 [3] with LEAP for an As implant in silicon. The composition range of applicability of the LEAP is evident. The agreement between SIMS and LEAP is excellent. Five different runs are overlaid to illustrate the reproducibility of the analysis.

Thickness metrology can be done with high precision if the specimen material displays known atomic planes in the 3D image. For example, silicon <100> oriented materials can be analyzed with a real space interatomic correlation routine called spatial distribution maps [9] that make it possible to use the atomic planes as an internal calibration standard. Figure 7 shows such an analysis for silicon. These analyses are most readily obtained for metals, but may not be observed in all materials of technological significance.

Specimen preparation is straightforward using state-of-the-art focused ion beam (FIB) tools equipped with micromanipulators to lift out items from structures. Site specificity can be as precise as ± 10 nm in three directions. Accuracy is determined by the visibility of a feature in the SEM or ion-induced image of the dual-beam FIB. A sequence of steps routinely used to extract devices from microelectronic structures is shown in Figure 8.

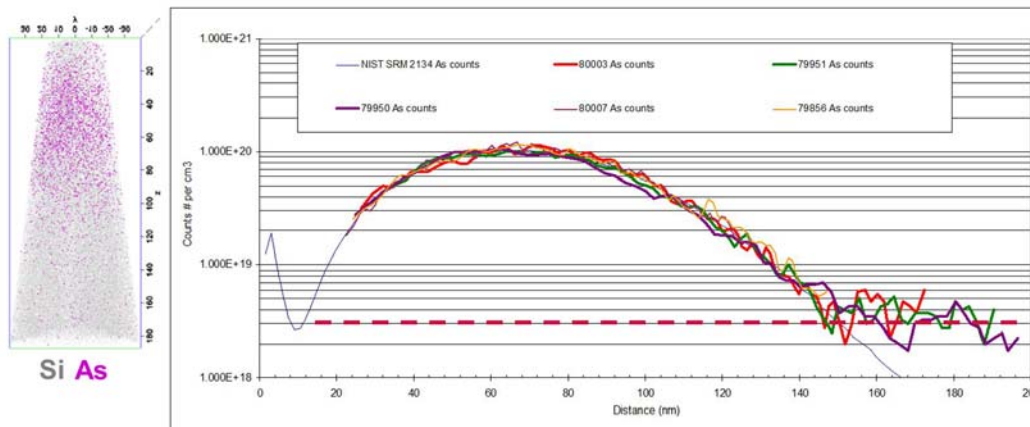


Figure 6 SIMS (Blue Curve) Analysis of NIST 2137 Compared with LEAP

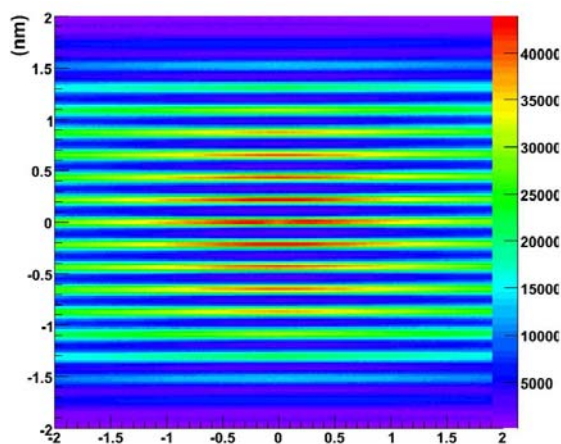


Figure 7 Spatial Distribution Map of a Silicon Specimen Showing the {200} as Horizontal Planes in the Data

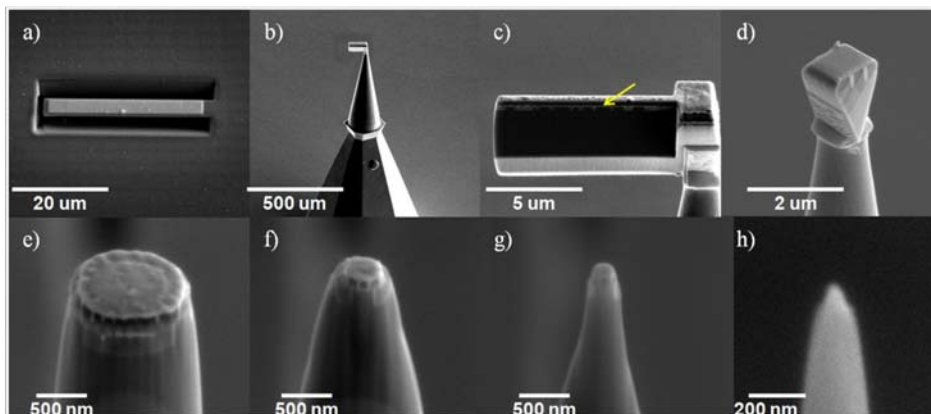
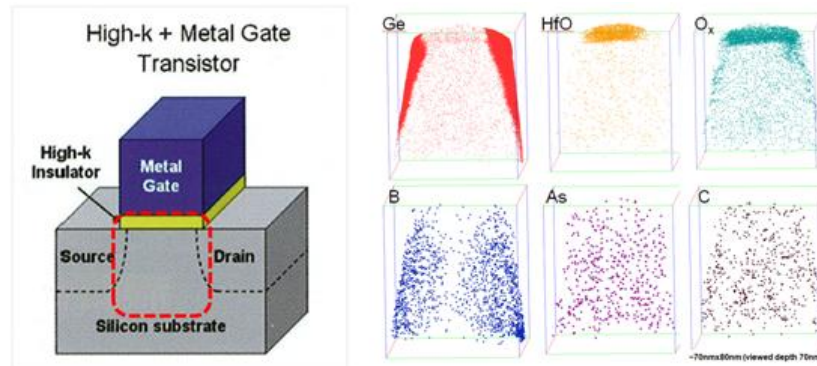


Figure 8 Stages of FIB Specimen Preparation from a) Cutting Trenches to h) Final Tip Shape

Figure 9 [10] shows a result from analyzing an off-the-shelf microprocessor (Intel i5-650) that was deprocessed before being lifted out of a transistor structure. The SiGe regions in the source/drain, the high-k gate dielectric, and the dopant atoms in the channel region are evident in the images on the right. This type of analysis, while meticulous today, should become routine in the next two years.



Reprinted with permission from the Microscopy Society of America and Cambridge University Press

Figure 9 Schematic of the Transistor and Atom Maps from a 20 nm Thick Segment of the Transistor Status of ISMI/SEMATECH-NIST XRR Standard Reference Material Development [10]

4.5 Calibration Artifact Development

Several approaches to calibration artifacts for XRR have been studied both at NIST and other National Metrology Institutes (NMIs). The simplest approach is a well characterized single layer material with minimal oxidation or interfacial diffusion over time. The thickness, roughness, and density of this layer could be modeled and compared using different commercial XRR measurement hardware and analysis software. This approach was first studied in 2000–2003 by the Physikalisch-Technische Bundesanstalt (PTB) using high quality pulse laser-deposited Pt on glass substrates. Since then, NIST has explored several materials as possible single layer or capped single layer structures. NIST has also collaborated with the National Metrology Institute of Japan (NMIJ) on data analysis approaches to address thickness uncertainty caused by surface contamination, one of the principle draw backs of using a single-layer structure. Figure 10 illustrates some of the pros and cons of a single layer SRM.

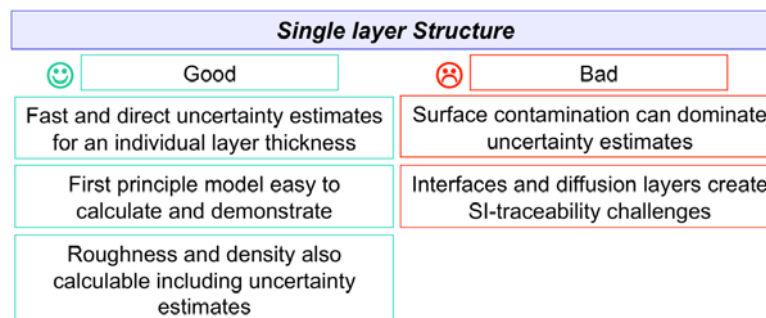


Figure 10 Pros and Cons of a Single Layer Structure as an XRR SRM

NIST and SEMATECH focused on direct thickness traceability using XRR. Using reference films of known thickness as an SRM, inter-tool thickness allows comparisons across tools and fabs.

NIST's SRM development often involves three independent research projects: calibration artifact development, SI-traceable instrumentation development, and data analysis and uncertainty determination. SEMATECH developed the thin film structures to serve as the calibration artifacts for this work.

In collaboration with ISMI and SEMATECH, NIST has explored several possible materials to-date. HfO_2 has great potential, due to its high-electron density contrast with Si. However, preliminary work with this material has yielded poor results due to potential film instability over time. For 2010, ISMI, SEMATECH, and NIST studied a Si_3N_4 single-layer film, working with an existing process recipe which provided very smooth, uniform films on Si. Figure 11 is a plot showing theoretical XRR data from the proposed 50 nm Si_3N_4 film.

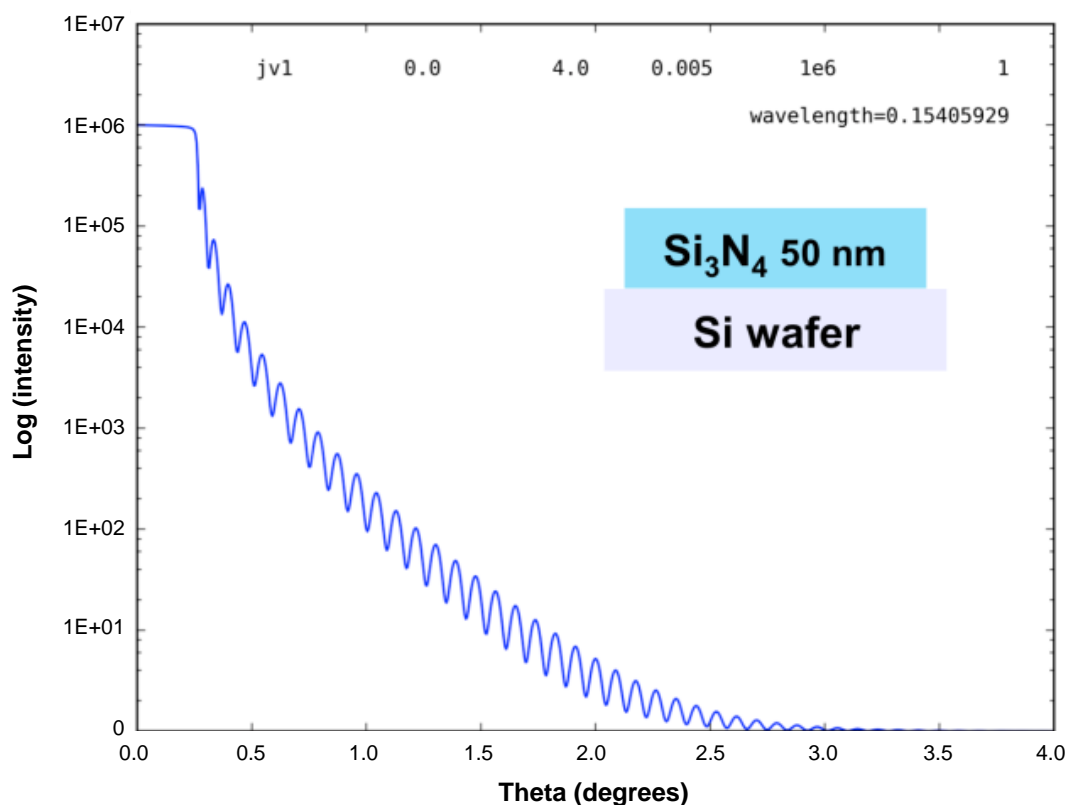


Figure 11 Theoretical XRR Data from a 50 nm Si_3N_4 Film on a Si Substrate

An alternative approach is to use a multilayer structure, which allows diffraction between the individual thin film layers. The diffraction features are usually more intense and sharper than features caused by the interference phenomenon from a single layer film. As an analogy, a multilayer structure provides a diffraction grating rather than a single slit for the X-ray measurement. The problem with this approach is that it introduces numerous free parameters and the information from all these parameters become convoluted within a single data file. Figure 12 details some of the pros and cons for multilayer structures as XRR calibration artifacts.

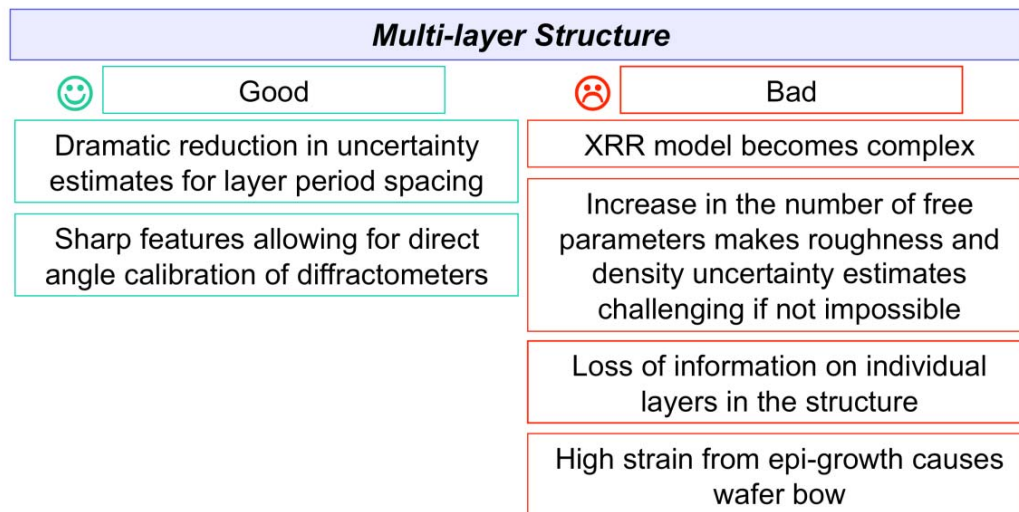


Figure 12 Pros and Cons of a Multilayer Structure as an XRR SRM

A SiGe superlattice structure was proposed for this initial phase of multilayer artifact design. Figure 13 shows the theoretical pattern from such a superlattice film. A three bi-layer design was used to compare with a similar GaAs/AlAs multilayer on GaAs developed by the NMIJ.

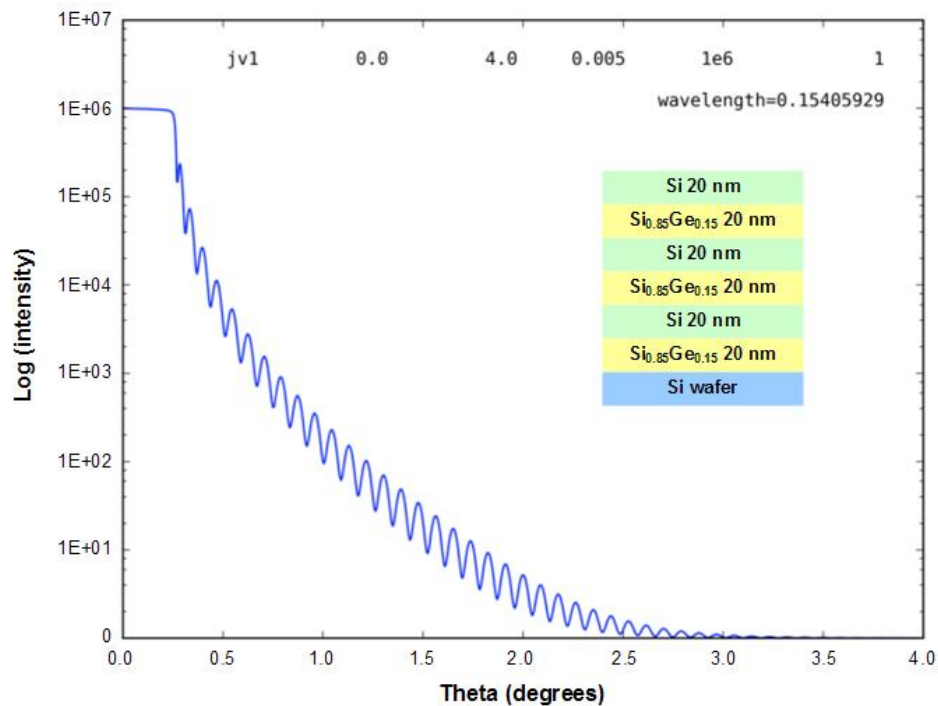


Figure 13 Theoretical XRR Data from a Three Repeat Bi-Layer Si/GiGe Structure on a Si Substrate

4.5.1 Data Analysis and Uncertainty Estimation

One of the most difficult problems with XRR is extracting structural information and its corresponding uncertainty from the data. In modeling terms, extracting structural model information from the data requires simulation of the data using parameter initial values and comparing the simulated data with measured data. Structural parameter values are then varied until the best fit or the smallest difference between the simulated and measured data is found. Figure 14 illustrates this process for XRR data analysis, which could be applied to nearly any form of data refinement.

In the late 1990s, a differential evolution approach (known as a genetic algorithm [GA]) was applied to determining the global minima in XRR data. Due to the interference of the measurement technique, the parameter solution spaces are filled with periodic structured local minima, often as convoluted and rich with features as the data itself. The GA approach involves taking a population of different structure parameter sets and solving for the difference between data and simulation for each member in a population. Then, only the fittest—typically the top half, best fitting members in the population—breed (mix structural model parameters) to produce another generation. The next generation repeats the process until a best fit is achieved. This approach is highly successful at finding an optimum solution to a complex structural model and finding a global minima in a sea of local minima. However, it fails to provide an estimate of the uncertainty of individual parameters within the best fit.

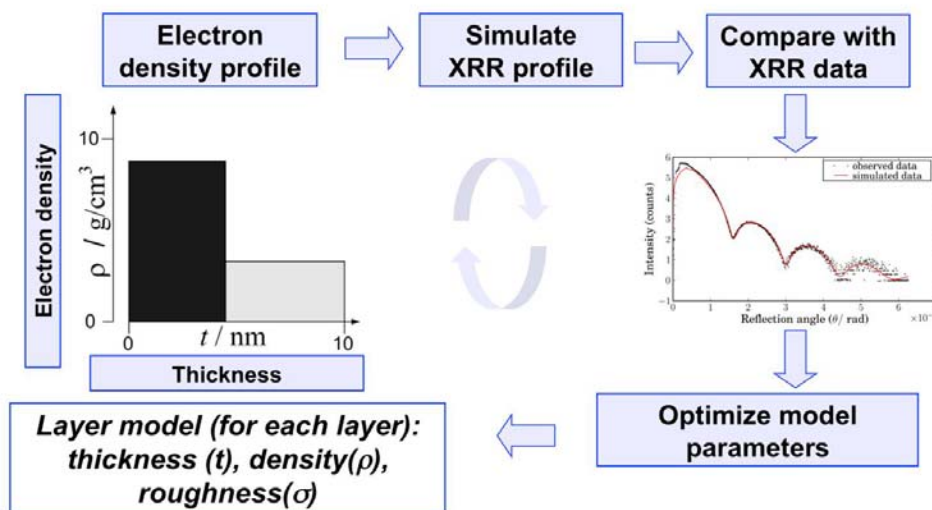


Figure 14 Data Analysis Method for Refining Physical Parameters to XRR Data

In the past five years, NIST has collaborated in the development of a Markov Chain Monte Carlo (MCMC) method to explore a statistical approach, rather than an optimization approach, to estimate parameter uncertainty. Monte Carlo simulations are time-consuming and require an in-depth knowledge of the types of noise within XRR data and of the underlying nature of the physical model. The MCMC approach allows for much faster data analysis than is possible with traditional Monte Carlo methods, but requires parameter tuning and frequent analysis reiterations. Despite such difficulties, the approach proves surprisingly robust in uncertainty estimation and answers some of the most perplexing questions in XRR data analysis: 1) what is the sensitivity of XRR for observing individual parameters? and 2) what are the uncertainty

estimates for each parameter within an analysis? Figure 15 compares GA and Monte Carlo approaches. Monte Carlo methods are slower than GAs because they have more parameters and are more difficult to implement because the complexity of the probability density function makes simple sampling approaches impractical.

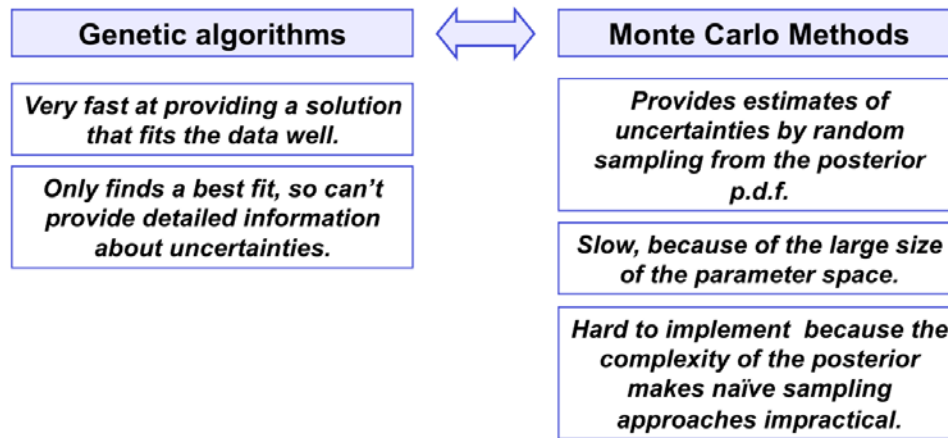
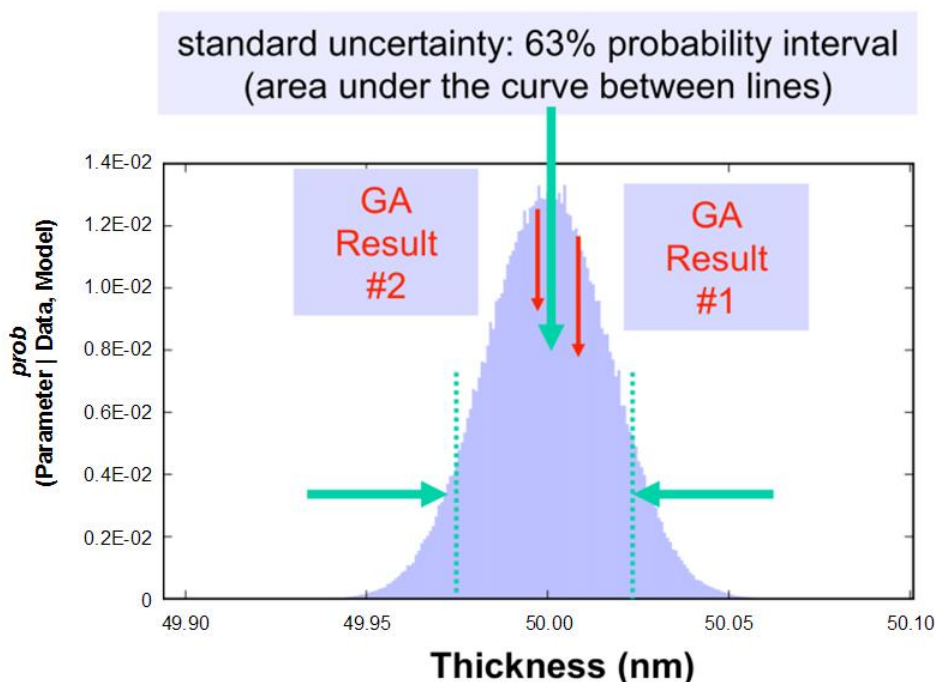


Figure 15 Comparison of Genetic Algorithms (optimization-based) vs. Monte Carlo (statistics-based) Data Analysis Methods

In Monte Carlo XRR analysis, a statistically large population of possible structural solutions is sampled and the corresponding likelihood is calculated for each solution. Previous information about the ranges for each parameter can be included in this analysis. Typically, a range of allowed values for each parameter is selected and all values over the range are assumed to be equally probable. The likelihood is selected through analysis of the sources of noise in the data. In XRR analysis, either log-normal or Poisson statistics are used in calculating the likelihood. The Markov Chain component is a method to actively sample more information from solutions near the optimum solution for the given model. The distances sampled for each parameter are then optimized such that ~25% of the time information is being gathered near optimum values. This approach allows a more comprehensive exploration of a high probability solution space with fewer total samples (faster results). The power of MCMC analysis is in developing probability distributions for any given parameter (over its range of allowed parameters) that are readily determined by overlaying the likelihood calculations for all samples in the statistically large data set. These probability distributions directly yield the statistical uncertainty of each parameter in the model, allowing Standard Uncertainty and Expanded Uncertainty to be determined through determining the 63% probability and 95% probability regions directly from the plots. Note that this represents the statistical uncertainty of the parameter from the XRR data analysis method. It does not include any of the Type B systematic errors from instrumentation and sample alignment and from instrument calibration. In this work, the total expanded uncertainty for a given parameter will always be larger than the stated values. Figure 16 shows the statistical posterior probability distribution calculated for a theoretical 50 nm Si₃N₄ film on Si. In comparison, GA analysis will give only a singular parameter value with no indication of the accuracy of the solution or an estimate of its uncertainty.



Note that the standard uncertainty (63% region) is shown along with various GA results.

Figure 16 Thickness Probability Distribution for Theoretical 50 nm Si_3N_4 on a Si Calibration Artifact

In analyzing XRR data, the physical structure is modeled using the electron density of the film and substrate as a function of depth. For this analysis, electron density scales well with mass density for light elements and is proportional in high density materials if the film stoichiometry remains relatively constant. Each new layer adds three parameters—thickness, density, and film roughness—to the analysis. The substrate is assumed to be of a known density and infinite thickness, leaving only substrate roughness to be modeled. Therefore, a single layer system requires modeling only four parameters. Film thickness is discussed here. Figure 17 shows the electron density for the theoretical Si_3N_4 film on Si. The height represents the density, the width the thickness. Roughness can be thought of as smoothing of the electron density edges in the transition regions.

For actual thin films, a surface contamination layer and possible interface between the substrate in the film often add complications. Each of these extra layers adds three free model parameters, turning a four parameter problem into a potentially ten parameter problem (Figure 18). When refining even single layer structures of XRR data, such elaborate models are sometimes necessary to provide a good fit to the measured data.

Electron density may also vary over the depth of the thin film. This gradient in electron density can be challenging to model, requiring many additional thin layers to approximate the gradient. Figure 19 shows such a gradient with the additional layers required to approximate it. Note that the solutions to the interference phenomenon used in the analysis consider only continuous density layers. This requires introducing a stack of varying density layers as the only way to model a gradient.

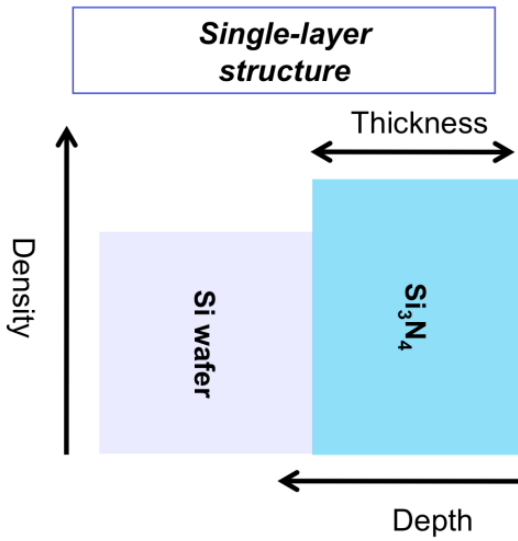


Figure 17 Electron Density of a Single Layer of Si₃N₄ on a Si Wafer

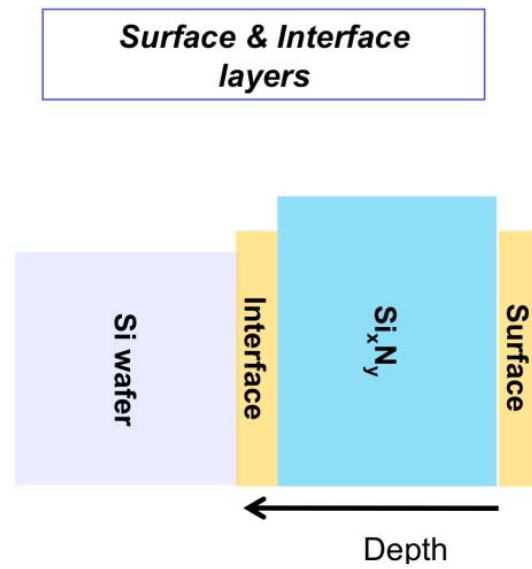


Figure 18 Electron Density of a Surface and Interface Layer for Si₃N₄ on a Si Structure

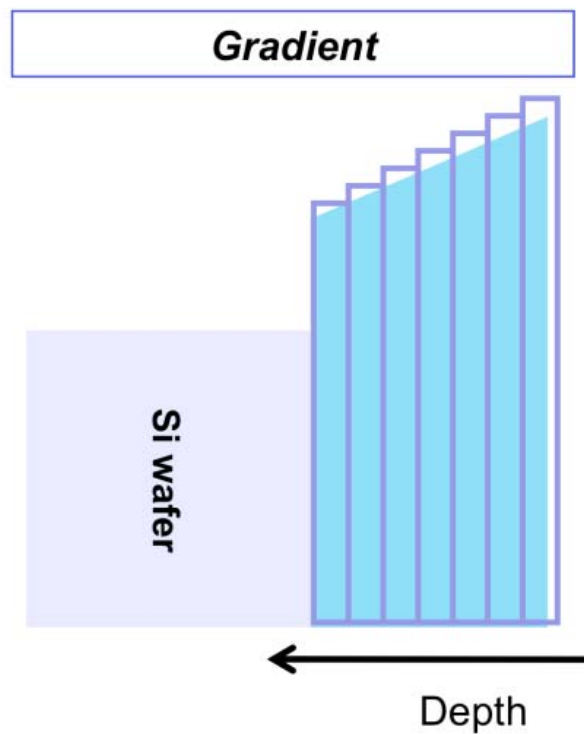
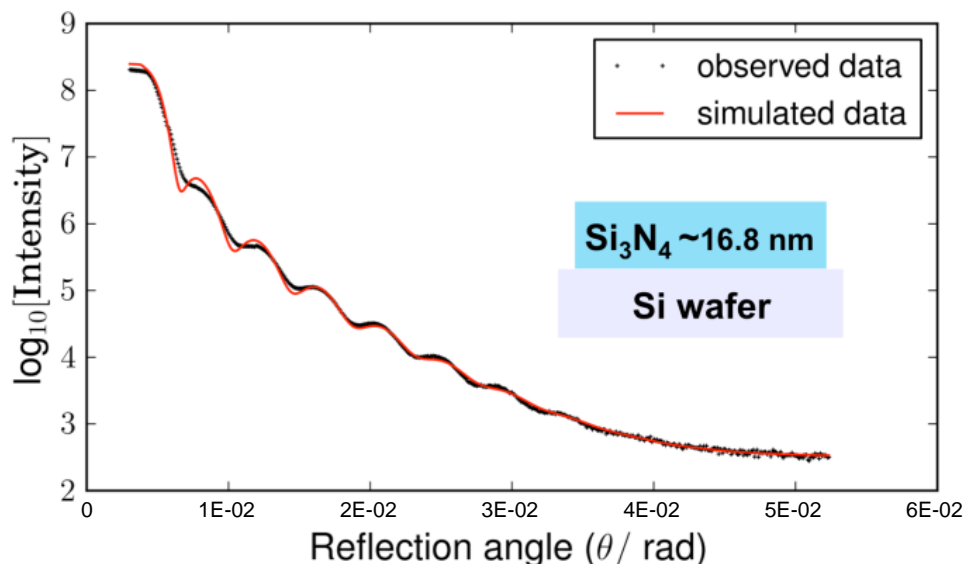


Figure 19 Electron Density for a Si₃N₄ Film with a Density Gradient

4.6 Results from Si₃N₄ Film XRR Data Analysis

SEMATECH deposited several Si₃N₄ thin films in 2010. A single furnace-deposited Si₃N₄ film, which was measured by XRR at SEMATECH directly after deposition, is presented here. The XRR data were analyzed at both SEMATECH (using GA) and at NIST (using GA and MCMC). A GA optimization result for a single layer model is shown in Figure 20. Note that the data and model agree in periodicity (film thickness) but not in peak shape. This indicates the need for a more complex model that includes either interfacial layers or a density gradient.

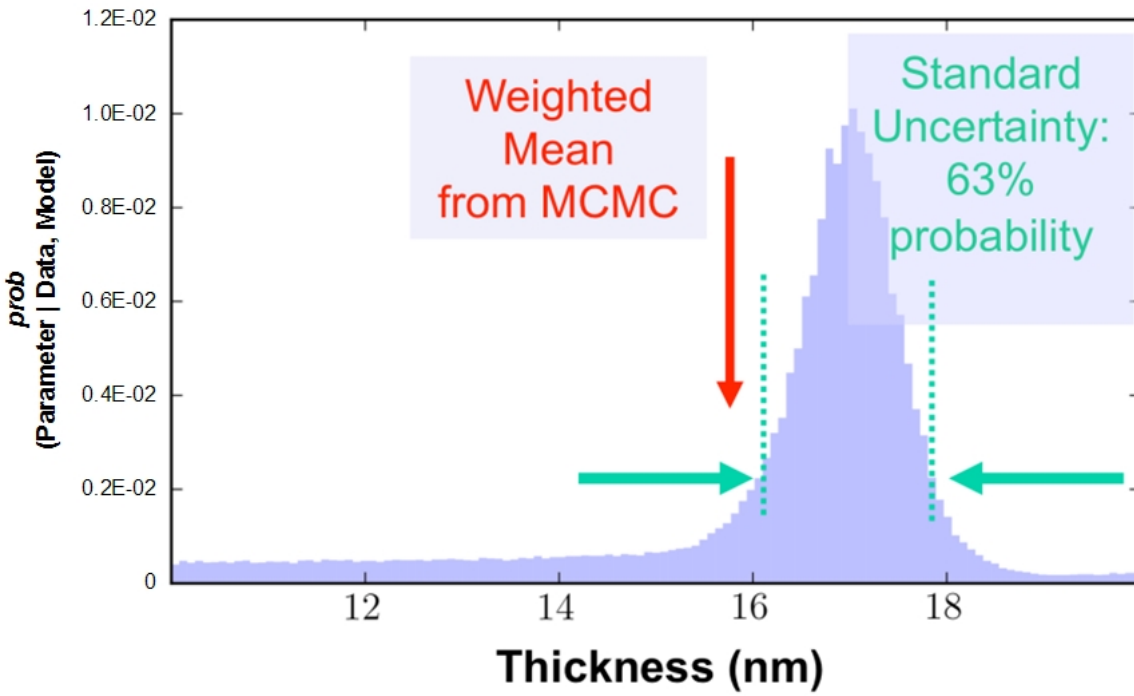


Note that the observed and simulated data do not agree. The actual data has weaker intensity oscillations than predicted by a single layer model.

Figure 20 Actual XRR Data from a 16 nm Si₃N₄ Film on a Si Substrate

To establish the robustness of XRR, Monte Carlo analysis was performed on the single layer model (see Figure 20) to find a consistent thickness determination from GA and Monte Carlo techniques for a range of different models. In the theoretical development of the structural model, a symmetric, Gaussian-shaped thickness probability density was predicted. Instead, a single layer model exhibits a Gaussian distribution superimposed with a nearly constant probability component over the entire previous range of allowed film thicknesses. The constant contribution is enough to move the weighted mean for the probability distribution outside the 63% probability estimation region (Figure 21).

An eight-layer model was developed with the central six layers fixed to 2 nm widths. The densities of all eight layers were allowed to float. The thicknesses of the first and last layer in the stack were also allowed to vary to refine the total cumulative thickness for the eight-layer system. Figure 22 shows the electron density profile determined using Monte Carlo analysis. The blue boxes are the high range and the grey boxes are the low range of the Standard Uncertainty (63% probability). The filled boxes are the weighted mean from the Monte Carlo statistics. This result offers strong evidence of a gradient within the Si₃N₄ film starting with high density at the film surface and becoming linearly less dense towards the Si substrate.



Note that the thickness probability extends into the low thickness region, decreasing the weighted mean and establishing a large expanded uncertainty (95% probability).

Figure 21 Thickness Probability Distribution for One-Layer Markov Chain Monte Carlo Analysis

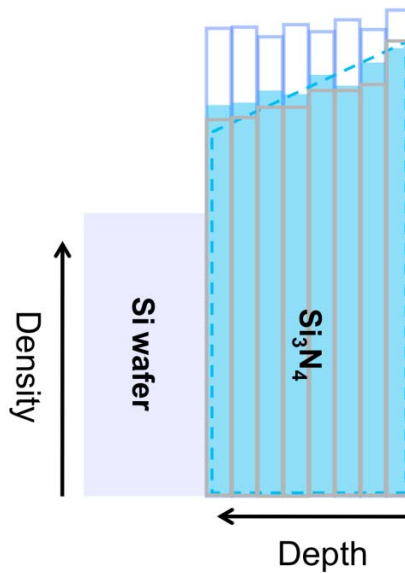


Figure 22 Electron Density for the Eight-Layer Monte Carlo Model of the Actual Si₃N₄ Film Data

The final experiment with this film was to establish the robustness of XRR to measure thickness, even with a pronounced density gradient. The film thickness determined using three different GA software packages and the GA and Monte Carlo results from the one-layer and eight-layer structural models was compared (Table 3). The one-layer GA results ranged between 16.71 nm and 16.86 nm. Thickness shows only a 0.26 nm total deviation across three different sets of analysis software, demonstrating the versatility of XRR for monitoring process variation. For the Monte Carlo and GA techniques, the Standard Uncertainty ranges rather than the weighted mean thickness from the Monte Carlo method need to be compared. The one-layer Monte Carlo provides a $17 \text{ nm} \pm 0.7 \text{ nm}$ range for Standard Uncertainty, which agrees well with the GA results, including the observed variance. The eight-layer model shows a somewhat lower thickness value from the Standard Uncertainties of $16.3 \text{ nm} \pm 0.5 \text{ nm}$. The GA result is slightly outside this range. However, Standard Uncertainty represents only 63% probability of the result being within the range of values.

Table 3 Thickness Determination Comparison for Furnace Si₃N₄ on Si (nominal 15 nm)

	Thickness	Standard Uncertainty K = 1 (63% probability)	Expanded Uncertainty K = 2 (95% probability)
SEMATECH 1 Layer (graded)	16.77 nm		
NIST 1 Layer (GA)	16.86 nm		
NIST 1 Layer (MCMC)	16.29 nm ^{***}	16.32–17.7 nm	10–18.7 nm*
NIST 1 Layer (GA ^{**})	16.71 nm		
NIST 8 Layer (GA)	16.86 nm		
NIST 8 Layer (MCMC)	16.18 nm ^{***}	15.83–16.84 nm	15.15–17 nm*

Note: The results represent the type A statistical uncertainties caused by XRR data analysis.

*95% probability regions may be larger than stated (ranges are exceeding modeling boundaries).

** Commercial software refinement for comparison.

*** Weighted mean values may be inappropriate, due to strong asymmetry in probability distributions.

5 CONCLUSION AND FUTURE DIRECTION

In 2010, several test structures were developed and the capability to model thickness information from both theoretical structures and deposited thin films was tested. Although Si₃N₄ forms smooth, uniform films, the density gradients within the film will make this material unsuited for an XRR SRM. Future work will analyze data from a multilayer structure deposited by SEMATECH in 2010 and will refine the calibration artifact design.

5.1 SEMATECH Reference Wafer Samples

A nominal 50 nm Si₃N₄ wafer was fabricated by chemical vapor deposition. The thickness was chosen to increase the number of XRR fringes observable in the sample to reduce measurement uncertainty.

Figure 23 illustrates the XRR simulation of the simple three-layer model (Table 4) for the Si₃N₄ wafer showing an increasing density as the film gets thicker, which is consistent with experimental results.

Table 4 Three-Layer Regression Model with 10 Parameters Floating

N	R	Material	Thickness	Roughness	Density T	Density N
1	1	SiN	2.5000	1.0000	4.00000	3.44000
2	1	SiN	50.0000	1.0000	3.40000	3.44000
3	1	SiN	2.0000	1.0000	3.00000	3.44000
SUB	1	Si	0.0000	1.0000	2.32910	2.32910

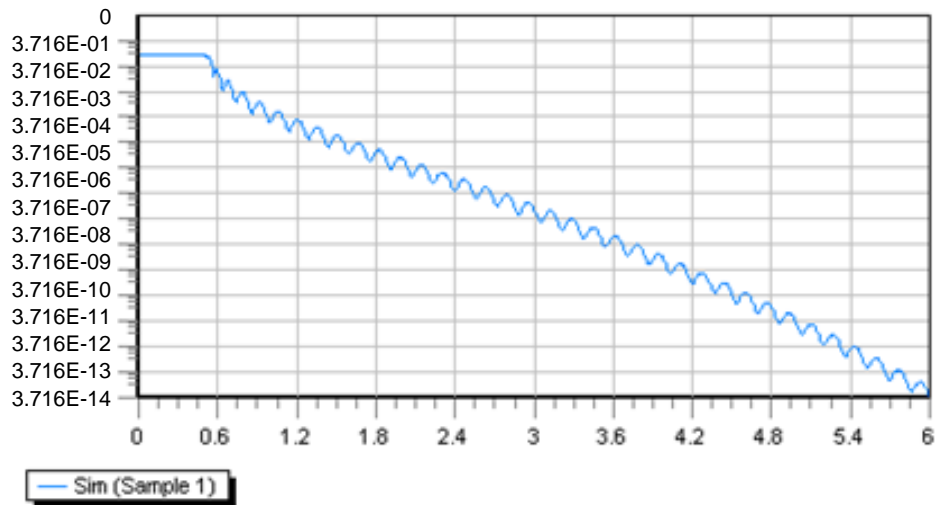


Figure 23 CVD Si₃N₄ Simulated Reflectance Spectrum

Figure 24 compares the modeled and measured results, showing the model is unable to correctly depict fringes at low reflectance angles. This is likely due to thickness variations at lower angles when the beam is longer. There is also a spectral mismatch at higher angle fringes, likely due to density variation that is not accounted for in the model.

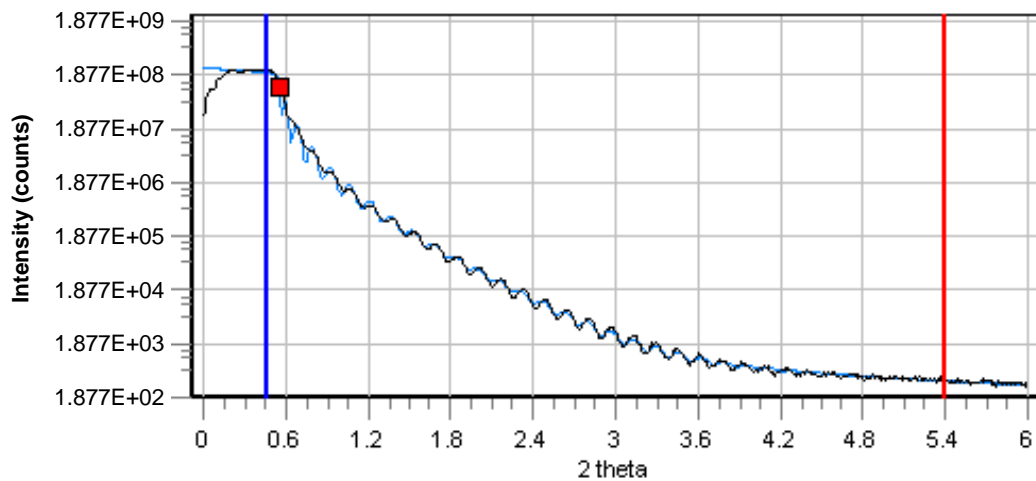


Figure 24 CVD Si₃N₄ Simulated and Measured Reflectance Spectra

A three-layer Si_3N_4 model was used to test density variation with depth, with the results of 200 iterations of a GA refinement shown in Table 6. A significant density gradient is shown, with a 30% vertical increase in density from bottom to top. Figure 25 is a topographical map for the total Si_3N_4 thickness, showing a 3 nm increase in film thickness from the 5 o'clock to 11 o'clock position, likely due to a showerhead pattern (the wafer is not rotated in the deposition tool). A $1-\sigma$ variation plot is shown in Figure 26.

Figure 27 is an 81-point topographical map of wafer thickness obtained using spectroscopic ellipsometry, verifying the XRR measurements in Figure 25. The spot sizes of SE and XRR vary significantly, as SE is on the order of $30\ \mu\text{m}$ and XRR is on the order of $50\ \mu\text{m}$ by up to 5 mm. XRR measurements thus encompass more film thickness variation (see Figure 2), and the fringe spacing can vary at small angles (low incident angle) to reflect this thickness variation.

Table 5 Results of Three-Layer GA Regression

N	R	Material	Thickness	Roughness	Density T	Density N
1	1	SiN	2.581	1.0460	4.12762	3.4400
2	1	SiN	47.9320	0.9991	3.44732	3.44000
3	1	SiN	2.2459	1.0259	3.08629	3.44000
SUB	1	Si	0.0000	0.9941	2.32910	2.32910

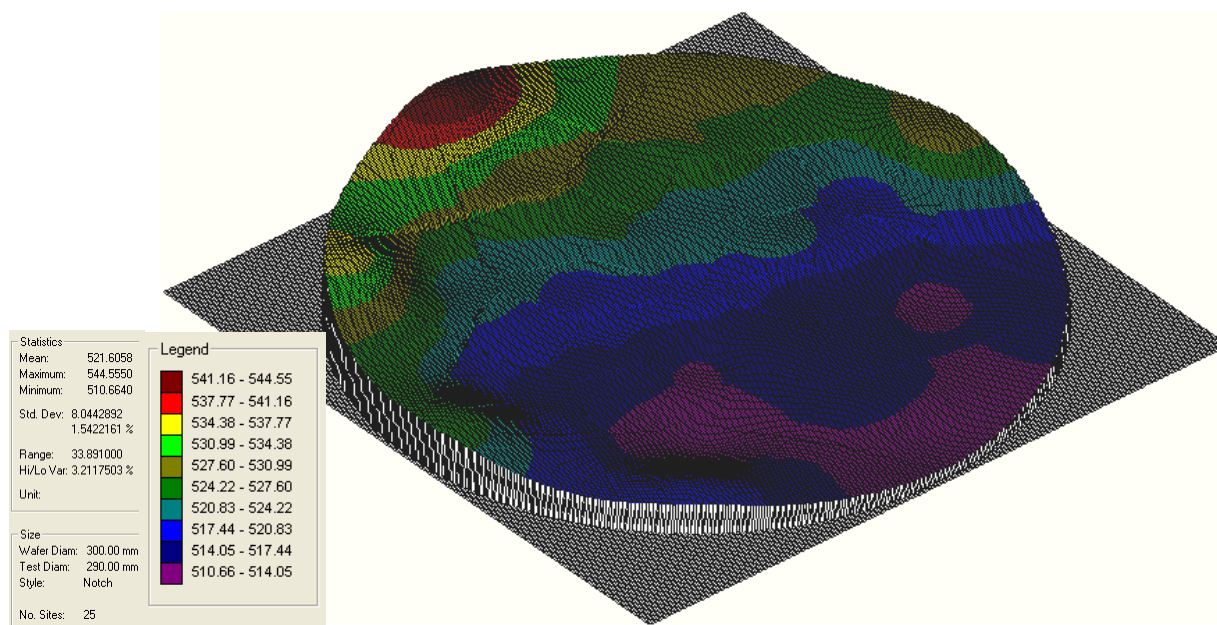


Figure 25 Topographical Map of 50 nm CVD Si_3N_4 Wafer

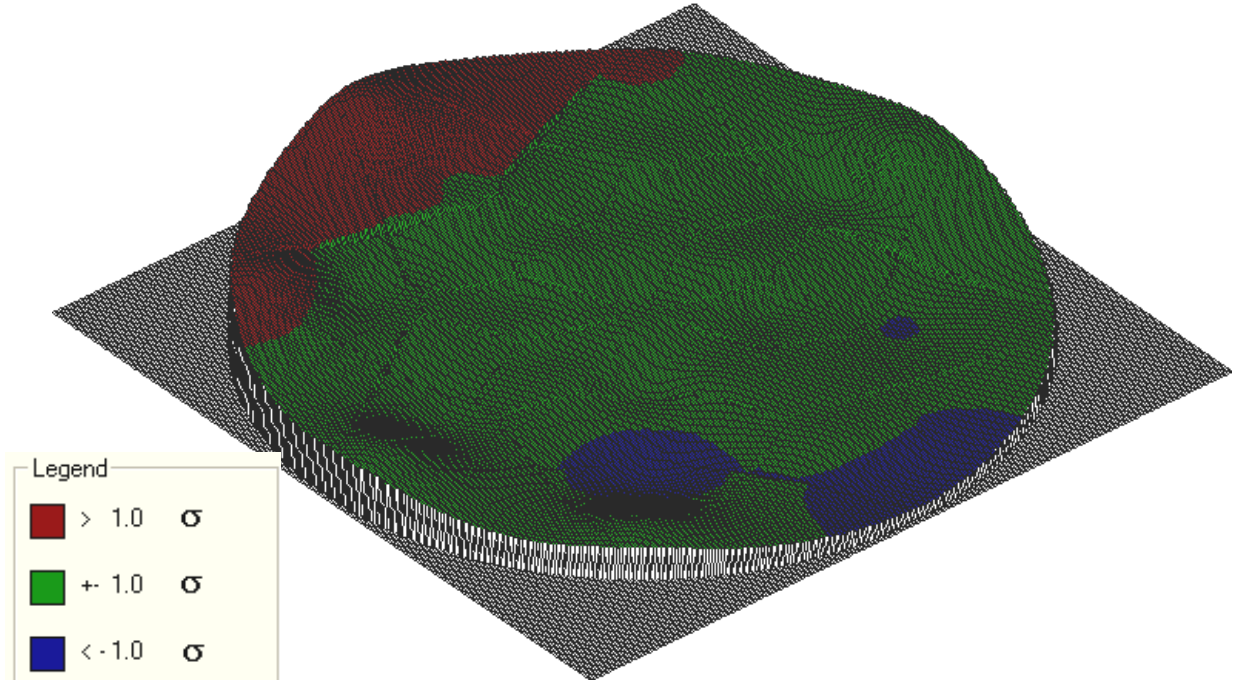


Figure 26 1- σ Topographical Map of Variation for the 50 nm CVD Si₃N₄ Wafer

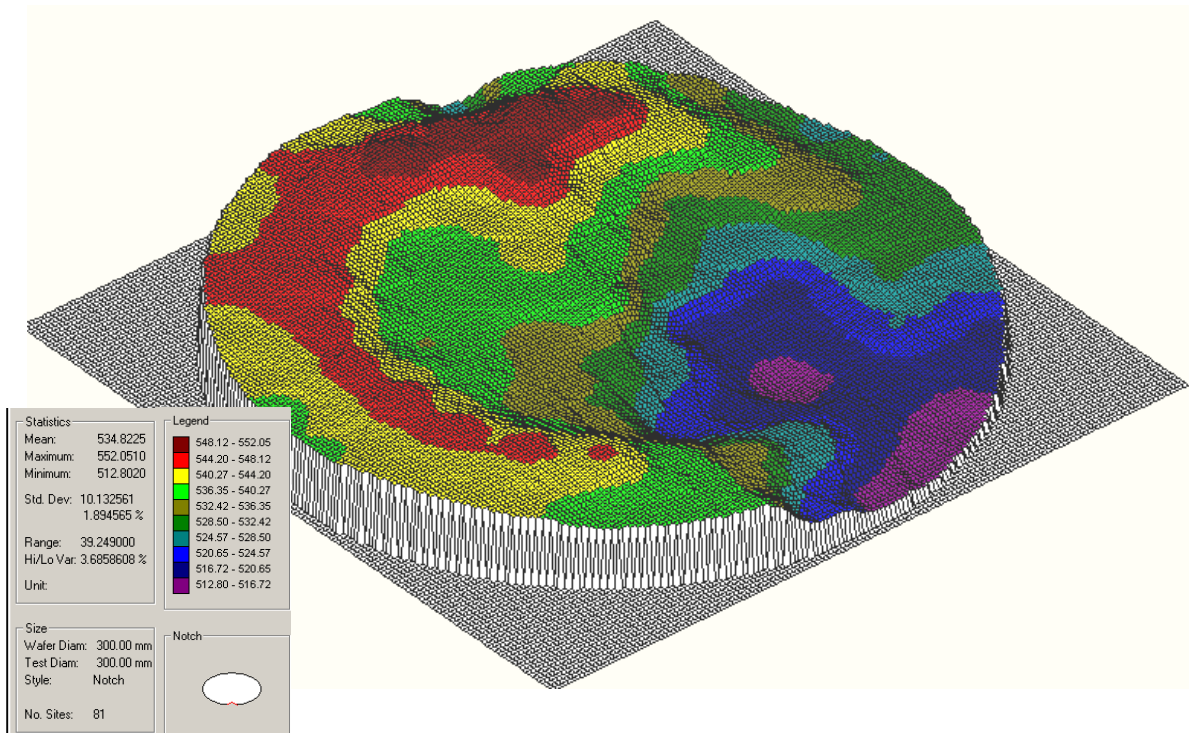


Figure 27 81-Point Spectroscopic Ellipsometry Surface Topographical Map of 50 nm CVD Nitride Film

As a possible route to a more uniform wafer (i.e., across-wafer thickness and depth-dependent density), a 15 nm Si_3N_4 wafer was fabricated in a silane furnace. A three-layer Si_3N_4 film was used in the GA refinement, as see in Table 6, but again density increased 20% as a function of depth.

Table 6 Three-Layer Regression Model with 10 Parameters Floating

N	R	Material	Thickness	Roughness	Density T	Density N	Density B	Profile
1	1	SiN	5.1933	0.7078	3.77283	3.4400	3.77283	No Gradient
2	1	SiN	5.7545	1.1030	3.48664	3.4400	3.48664	No Gradient
3	1	SiN	5.8351	0.9745	3.19440	3.44000	3.19440	No Gradient
SUB	1	Si	0.0000	1.0816	2.32910	2.32910	2.32910	No Gradient

The actual and modeled results of a three-layer GA model are shown in Figure 28 for the 15 nm Si_3N_4 wafer, highlighting that the model could not refine the first three fringes.

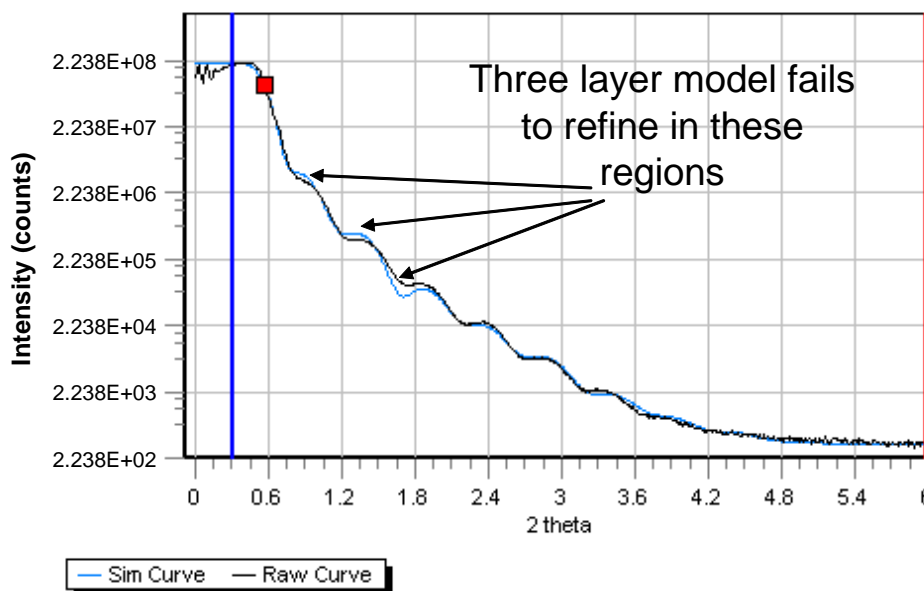


Figure 28 XRR Measured and Theoretical Reflectance Spectra Using a Three-Layer Model

An eight-layer model varying 25 parameters was used to more accurately model the film. The good agreement between the XRR data and model results in Figure 29 demonstrate the increase in density in just a 15 nm layer.

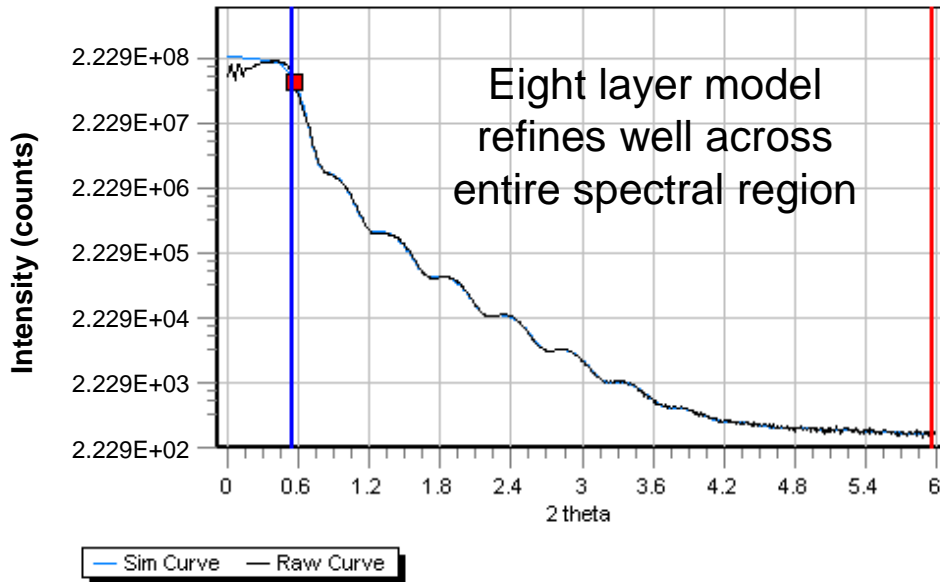


Figure 29 XRR Measured and Theoretical Reflectance Spectra Using an 8-Layer Model

A model with 25 free parameters is excessive, since the parameters are likely to correlate with one another. In practice, a maximum of 12 parameters is reasonable. Fixing the roughness for the center six layers is probably reasonable. The eight-layer model indicates an even higher Si_3N_4 density gradient than the three-layer model, with a 41% increase in density from layer 1 to layer 8, as shown in Table 7. Figure 30 is a topographical map showing the 0.8 nm range of the of the 15 thick nm Si_3N_4 wafer.

Table 7 Eight-Layer Regression Parameter Model with 25 Parameters Floating

N	R	Material	Thickness	Roughness	Density T	Density B	Profile
1	1	SiN	3.9908	1.0962	3.87006	3.87006	No Gradient
2	1	SiN	1.9589	1.0061	3.76090	3.76090	No Gradient
3	1	SiN	2.0706	0.9564	3.71113	3.71113	No Gradient
4	1	SiN	1.9380	1.2864	3.55894	3.55894	No Gradient
5	1	SiN	1.8756	1.1545	3.45091	3.45091	No Gradient
6	1	SiN	1.8870	1.1122	3.31107	3.31107	No Gradient
7	1	SiN	2.4764	1.0797	3.15444	3.15444	No Gradient
8	1	SiN	0.9767	1.0191	2.74474	2.74474	No Gradient
SUB	1	Si	0.0000	0.9207	2.32910	2.32910	No Gradient

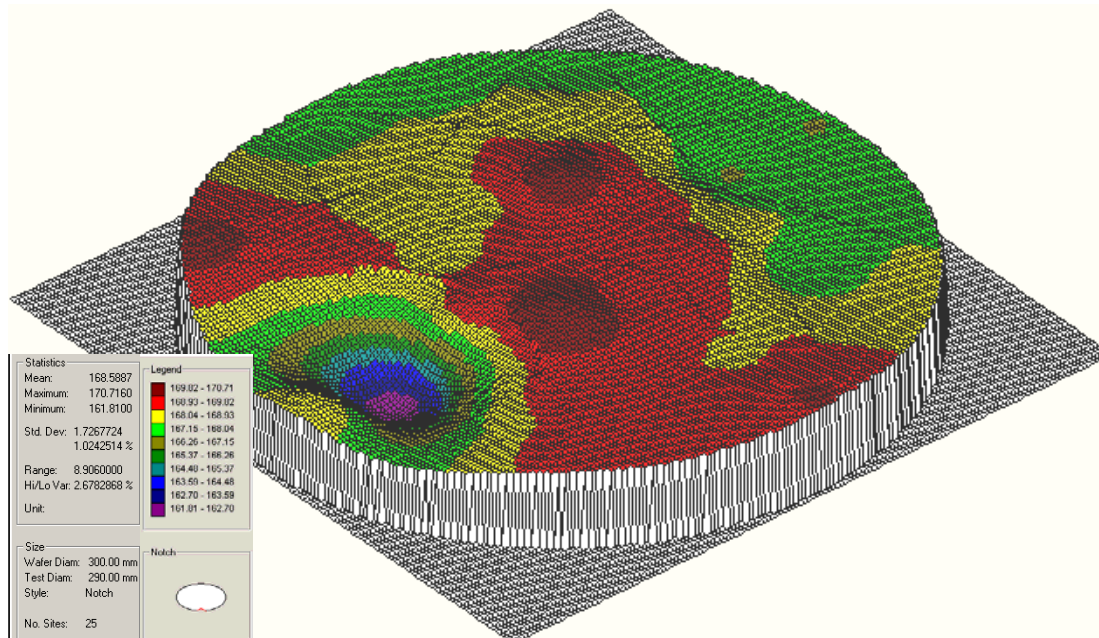


Figure 30 25-Point XRR Surface Topographical Map of the 15 nm CVD Nitride Wafer

A $1\text{-}\sigma$ topographical map of variation for the furnace-deposited 15 nm Si_3N_4 wafer is shown in Figure 31, indicating that the majority of the wafer is within a $1\text{-}\sigma$ thickness range.

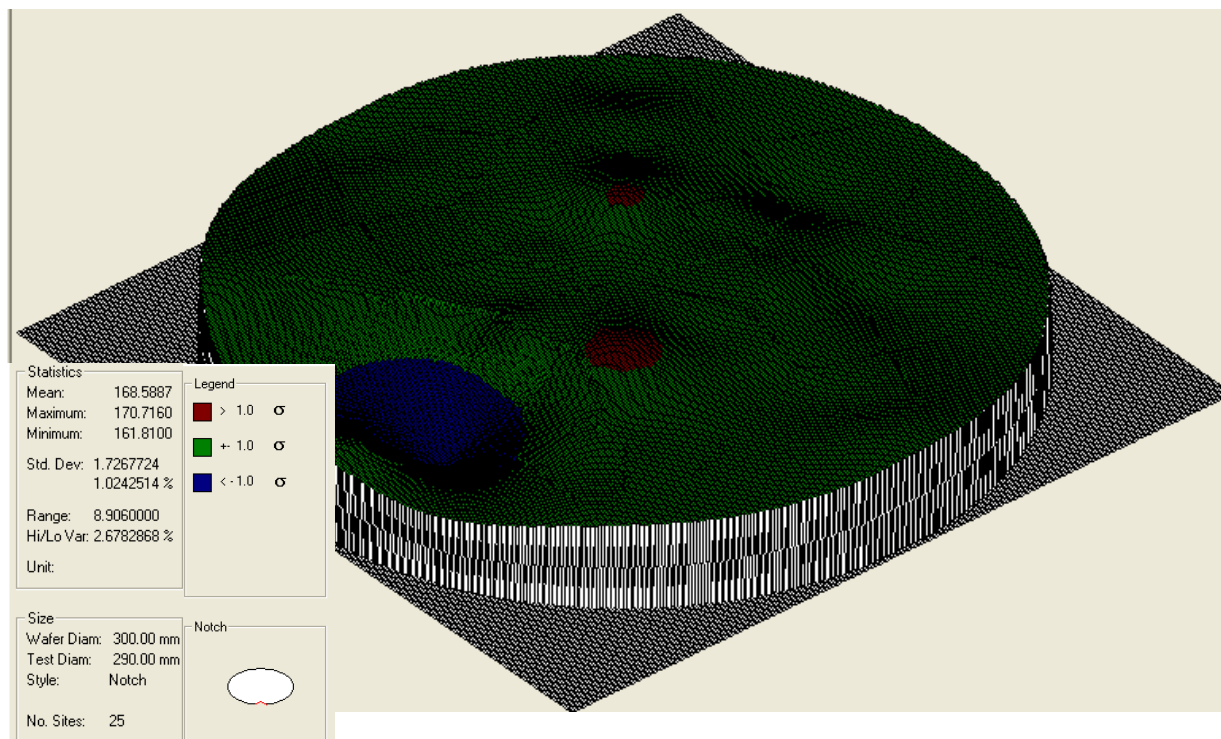


Figure 31 $1\text{-}\sigma$ Topographical Map of Variation for the Furnace-Deposited 15 nm Si_3N_4 Wafer

A SiGe/Si superlattice with a Si₃N₄ cap to prevent Si oxidation was also grown with recipes that were readily available, resulting in the film stack in Figure 32. A superlattice structure exhibits a number of sharply defined spectral features that would enable highly accurate thickness measurements, as shown in Figure 33.

A 15-parameter regression model as shown in Table 8 was used; the resulting spectra are compared with the actual data in Figure 34.

NIST has proposed a more complex SiGe superlattice (Figure 35) to be used primarily for TEM/XRR calibration. A simpler variant of the structure will be fabricated and evaluated in 2011.

Table 8 Regression Model with 15 Parameters Floating

N	R	Material	Thickness	Roughness	Density T	Density B	Density N	Profile
1	1	SiN	14/1140	0.7757	3.64916	3.64916	3.4400	No Gradient
2	1	SiN	16.9350	0.4976	2.81181	2.83181	2.32910	No Gradient
3	1	SiN	30.2384	0.2145	3.37417	3.37417	3.82742	No Gradient
4	1	SiN	18.9775	0.1813	2.66073	2.66073	2.32910	No Gradient
5	1	SiN	32.9088	0.6002	3.30173	3.30173	3.82742	No Gradient
SUB	1	Si	0.0000	1.0000	2.32910	2.32910	2.32910	No Gradient

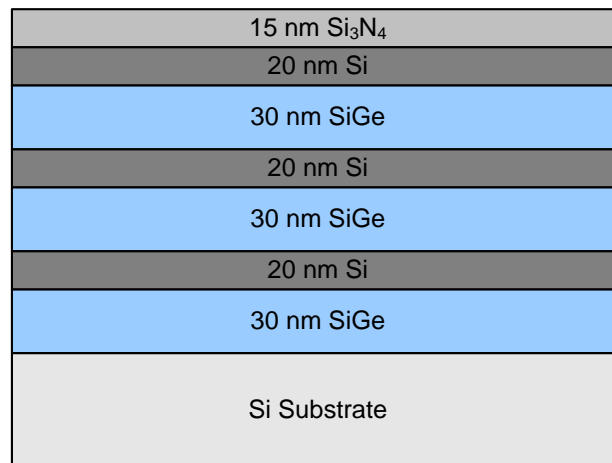


Figure 32 Illustration of SiGe Superlattice with Si₃N₄ Cap

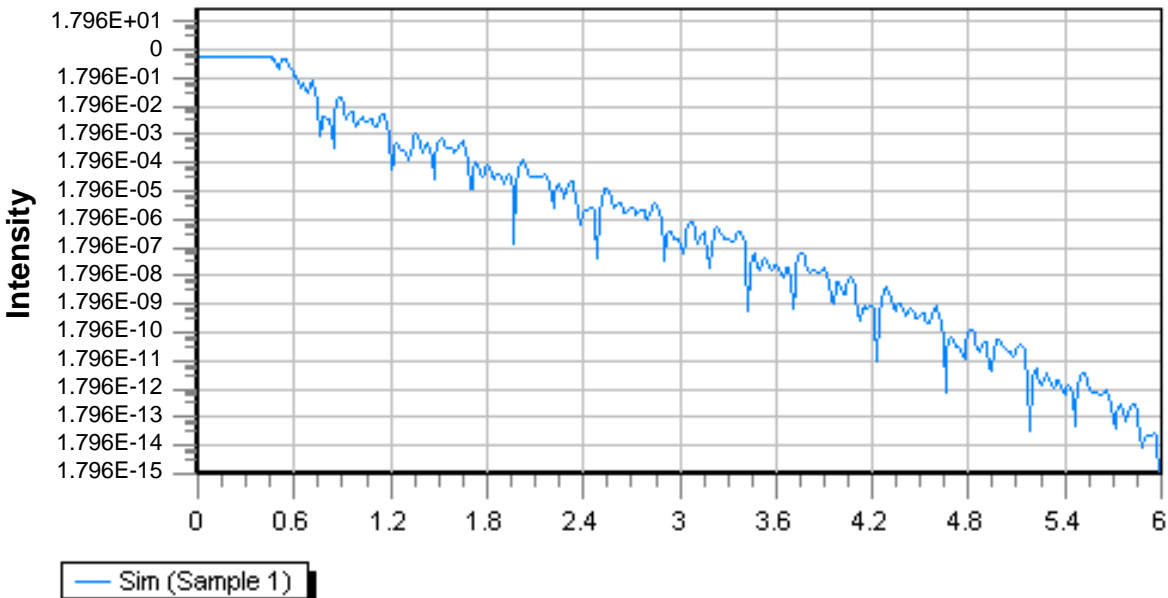


Figure 33 SiGe Superlattice Simulated Reflectance Spectrum



Figure 34 SiGe Superlattice Actual Reflectance Spectrum

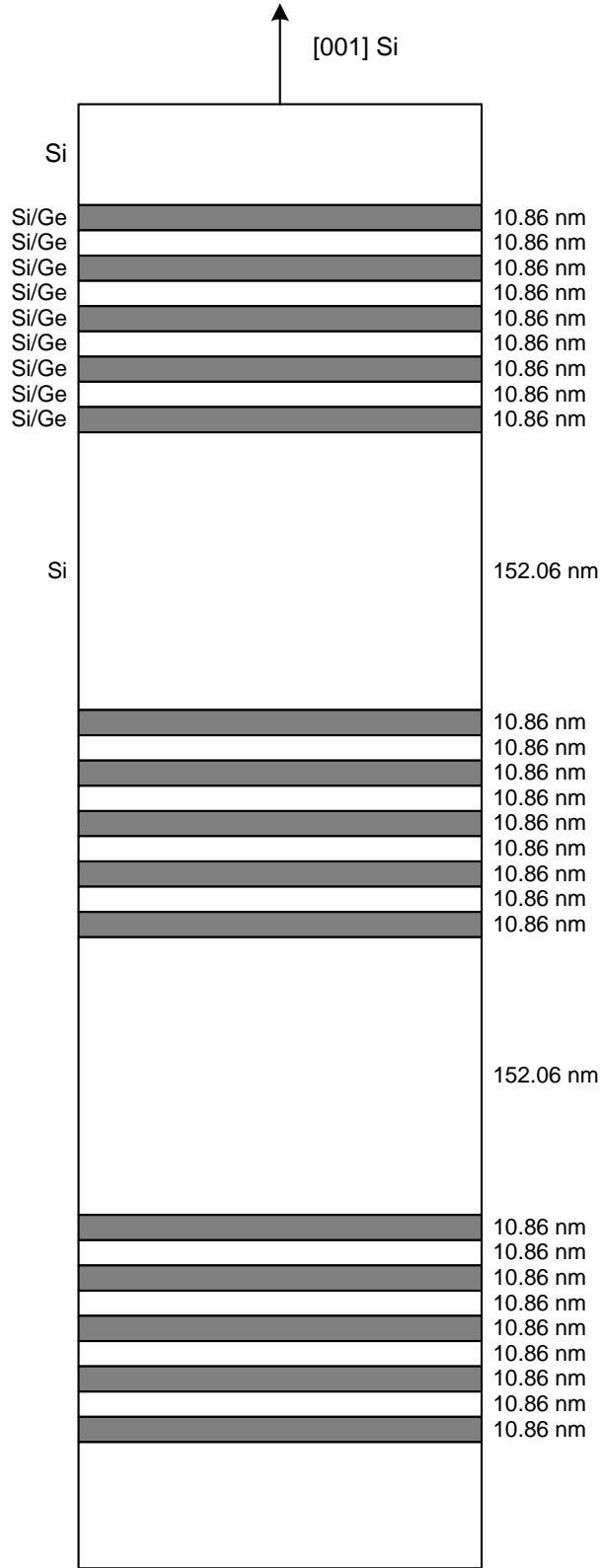


Figure 35 NIST-proposed Structure for Combined X-ray and TEM Calibration with Si/Si(1-x)Ge_x Strained Superlattices

5.2 Discussion

After appropriate single or multilayer wafers are fabricated and their time-invariance is verified, wafers will be sent to NIST for further measurement and uncertainty analysis of the primary films, interfaces (if any), and surface contamination. Spectral changes after longer periods of time (stability for more than two years desirable) or sensitivity to surface contamination from AMCs will also be measured, and their effects on uncertainty determined. An XRR standard requires a low roughness (<0.5 nm), high density film (10–20 nm) from a uniform process (such as atomic layer deposition) with sharp interfaces (no interdiffusion) and high density contrast, with a well-characterizable, robust process (e.g., SiO_2 , HfO_2 , Si_3N_4 , or TiN). A capping layer is beneficial to assure stability.

For an XRD standard, a stable, epitaxial layer on a Si substrate is desirable, since the Si lattice position must be included as a reference peak in the spectra. The films must have low defectivity (high crystalline quality), using a well known and well characterized structure, such as SiGe.

After analysis, wafers are typically diced into 25 mm x 25 mm squares or distributed as whole wafers to members of the X-ray community for use and feedback on their performance as reference materials. NIST certification of the SRM would then follow at a later date.

5.3 Conclusions and Outlook

Several techniques were evaluated for their suitability as first principles measurement techniques for thickness and composition metrology derived from the SI measurement standards of time and distance.

In 2010, SEMATECH developed and evaluated several thickness and composition test structures were. Thickness standards comprised of Si_3N_4 , a SiGe/Si lattice, and HfO_2/TiN were fabricated. In addition, B-doped SiGe and SiC wafers were fabricated as compositional standards.

The ability to model films by correlating theoretical structures to actual deposited thin films measurements by XRR was tested, and the quality of the films evaluated. Results by XRR were not promising, primarily due to density gradients as a function of depth.

XRR, XRD, XPS, and APT, with RBS and TEM for verification, are considered the best currently available methods for thickness and compositional reference metrology, with XRR, XRD, XPS, and APT being the primary methods used in this work.

Work will continue in 2011 to fabricate and evaluate films (B-doped SiGe, SiGe/Si superlattice, SiC) for thickness and composition reference standards. Wafers will be sent to NIST for further evaluation. The report will be updated at that time.

6 REFERENCES

- [1] *NIST SI-traceable X-Ray Reflectometry (XRR) Standard Reference Material Development*, A. Henins, D. Black, D. Windover, D.L. Gil, J.P. Cline, K. Mullen, ISMI Metrology Integrated AMAG/DMAG/FMAG Meeting - ISMI Litho Metrology Program Update - 7-8 October 2010, SEMATECH Pub: 35873.
- [2] "Invited Review Article: Atom Probe Tomography," Thomas Kelly, Michael Miller, *Review of Scientific Instruments*, 78, 031101 (2007).

- [3] D.S. Simons, P.H. Chi, R.G. Downing, and G.P. Lamaze, “The Development of Standard Reference Material 2137 – A boron implant in Silicon Standard for Secondary Ion Mass Spectrometry, in Semiconductor Present Status and Future Needs,” editors W.M. Bullis, D.G. Seiler, and A.C. Diebold, *AIP Press*, 1996, p. 382.
- [4] *NIST SI-traceable X-Ray Reflectometry (XRR) Standard Reference Material Development*, A. Henins, D. Black, D. Windover, D.L. Gil, J.P. Cline, K. Mullen Metrology Program Advisory Group (MET PAG), 19 Oct 2010, SEMATECH publication 35832.
- [5] Donald Windover, private communication.
- [6] L. G. Parratt, *Phys. Rev.* 95, 359 (1954).
- [7] <http://srdata.nist.gov/xps/DataDefinition.aspx>.
- [8] https://www.nist.gov/srmors/view_detail.cfm?srm=2841.
- [9] “Spatial Distribution Maps for Atom Probe Tomography,” B. P. Geiser, T. F. Kelly, D. J. Larson, J. Schneir, and J.P. Roberts, *Microscopy and Microanalysis* 13(6) (2007) 437-447.
- [10] “Prospects for Atom Probe Tomography of Commercial Semiconductor Devices,” D.J. Larson, D. Lawrence, D. Olson, T.J. Prosa, D.A. Reinhard, R.M. Ulfing, P.H. Clifton, J.H. Bunton, D. Lenz, J.D. Olson, L. Renaud, I. Martin and T.F. Kelly, *Microscopy and Microanalysis 2011 Conference*, accepted for publication.

**SEMATECH Technology Transfer
257 Fuller Road, Suite 2200
Albany, NY 12203**

**<http://www.sematech.org>
e-mail: info@sematech.org**